CHALMERS

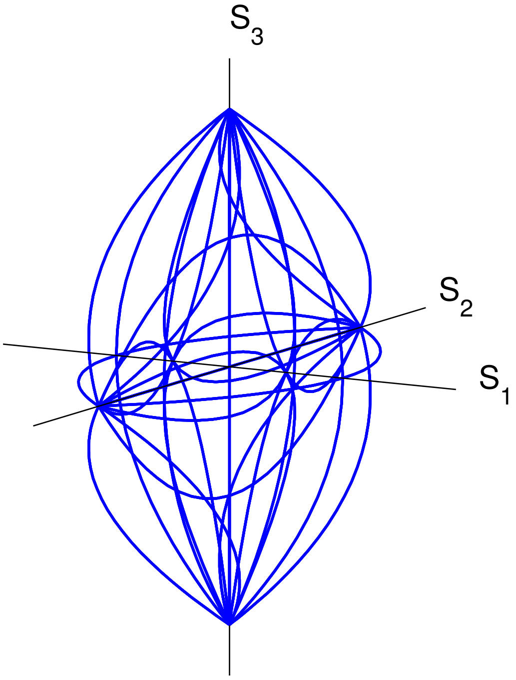

An In-Band OSNR Monitoring Method for Polarization Multiplexed QPSK Signals Using Stokes Parameters

Master's Thesis in Photonics Engineering

LARS LUNDBERG

EXFO Sweden AB

Department of Microtechnology and Nanoscience
Photonics Laboratory
CHALMERS UNIVERSITY OF TECHNOLOGY
Gothenburg, Sweden 2013

Master's Thesis in Photonics Engineering

An In-Band OSNR Monitoring Method for Polarization Multiplexed QPSK Signals Using Stokes Parameters

Lars Lundberg

EXFO Sweden AB
Arvid Hedvalls Backe 4

Department of Microtechnology and Nanoscience
Photonics Laboratory
CHALMERS UNIVERSITY OF TECHNOLOGY
Gothenburg, Sweden 2013

An In-Band OSNR Monitoring Method for Polarization Multiplexed QPSK Signals Using Stokes Parameters

Lars Lundberg

Photonics Laboratory
Department of Microtechnology and Nanoscience
Chalmers University of Technology
SE-412 96 Göteborg
Sweden
Telephone: +46 (0)31-772 10 00

Cover: The Stokes space representation of a polarization multiplexed QPSK signal.

Printed in Sweden by Reproservice, Chalmers Tekniska Högskola, 2013

Abstract

The optical signal-to-noise ratio (OSNR) is an important parameter for measuring signal quality in optical communications systems. Due to the recent development of polarization multiplexed systems, Nyquist filtered systems and reconfigurable systems, the traditional optical spectrum analysis method for estimating the OSNR cannot be used. Several other methods have been proposed, with various shortcomings, so there is a need for other methods.

In this work, an in-band OSNR monitoring method for polarization multiplexed signals based on a Stokes polarimeter has been investigated through theoretical studies, simulations and measurements. For the measurements, a 90° hybrid based polarimeter was constructed and used for measurements on noise loaded 28 GBd DP-QPSK signals. The impact of chromatic dispersion (CD) and polarization-mode dispersion (PMD) on the method was also investigated.

The method was successfully used to estimate the OSNR within ±1 dB for OSNR values up to 25 dB. Through simulations it was shown that the tolerable amount of CD increased if the bandwidth used for the ADC was decreased. In the measurements of this work, a bandwidth of 10 MHz was used, which should tolerate over 1000 km of SMF with $D = 17\,\mathrm{ps/nm/km}$ according to the simulations. However, the method was shown to be sensitive to PMD, tolerating a differential group delay of less than a tenth of the symbol time. Also developed in this work was a method for compensating for a non-ideal 90° hybrid.

A provisional patent application has been filed for the method.

Acknowledgements

I am very grateful to have had the opportunity to work on this interesting project at EXFO. I would like to thank my supervisor Henrik Sunnerud at EXFO for suggesting the project, and for his support and advice during the project, with many helpful discussions. I would also like to thank my examiner, Pontus Johannison at the Photonics laboratory, who has been a second supervisor helping me with both the project work and the report. Finally, I would like to thank all of the crew at EXFO for the friendly and welcoming atmosphere.

Lars Lundberg, November 2013

Contents

1 Introduction **1**

2 Background **3**
- 2.1 Optical modulation . . . 3
  - 2.1.1 A DP-QPSK modulator . . . 4
- 2.2 Optical signal-to-noise-ratio . . . 5
  - 2.2.1 Monitoring methods . . . 5
- 2.3 Other signal impairments . . . 6
  - 2.3.1 Chromatic dispersion . . . 6
  - 2.3.2 Polarization-mode dispersion . . . 7

3 The Stokes polarimeter OSNR monitor **9**
- 3.1 Theoretical background . . . 9
  - 3.1.1 Polarized light and the Stokes parameters . . . 9
  - 3.1.2 Representation of a modulated signal . . . 10
  - 3.1.3 Polarization of the signal . . . 11
  - 3.1.4 Noise in Stokes space . . . 11
- 3.2 Implementation and practical issues . . . 13
  - 3.2.1 Principle of operation . . . 13
  - 3.2.2 Hybrid imperfections . . . 14
  - 3.2.3 Tracking of polarization state and phase differences . . . 15

4 Simulations **17**
- 4.1 Method . . . 17
  - 4.1.1 Signal model . . . 17
  - 4.1.2 ASE model . . . 17
- 4.2 Results . . . 18
  - 4.2.1 Bandwidths and pulse shapes . . . 19
  - 4.2.2 Chromatic dispersion . . . 21
  - 4.2.3 Polarization mode dispersion . . . 21
  - 4.2.4 Other signal impairments . . . 24

5 Experiments **25**
- 5.1 Polarimeter setup . . . 25
  - 5.1.1 Digital signal processing . . . 26
- 5.2 OSNR measurements . . . 27
  - 5.2.1 Transmitter setup . . . 27
  - 5.2.2 OSNR estimation . . . 28
  - 5.2.3 PMD . . . 31
  - 5.2.4 Other experiments . . . 32
  - 5.2.5 Comparison with simulation results . . . 32

6 Conclusions 35

Bibliography 38

1 | Introduction

FIBER OPTICAL COMMUNICATION systems are an important part of the communication infrastructure of the world, and are responsible for the major part of international communication. During the last three decades the area has undergone a rapid progression, with an increase in the bit-rate by a factor of 100000 [1]. Among the key innovations making this possible is the erbium doped fiber amplifier (EDFA), the use of wavelength division multiplexed systems (WDM) and the introduction of coherent receivers and advanced modulation formats such as M-ary phase shift keying (M-PSK) and quadrature amplitude modulation (M-QAM).

In optically amplified links, the optical signal-to-noise ratio (OSNR) is an important measure of the signal quality [2]. Each amplifier the signal passes along the link adds noise and degrades the OSNR. The traditional method for measuring the OSNR with an optical spectrum analyzer (OSA) utilizes the linear interpolation technique to measure the noise power between the WDM channels. However, the recent advent of extremely densely packed WDM systems, Nyquist WDM systems [3] and reconfigurable systems have created a need for other methods, as the signal cannot be measured with the interpolation technique in these systems. Several methods have been proposed, among them a method based on the analysis of the Stokes parameters developed at EXFO Sweden AB. A similar method is also proposed by [4], where an integrated Stokes polarimeter is presented. However, the method has not been thoroughly investigated theoretically nor has it been shown that it can be implemented using readily available lumped components.

The purpose of this project is to further study the Stokes polarimeter OSNR measuring method. This includes developing the necessary theory for describing the method, implementing the method with a 90° hybrid polarimeter and investigating the effects of various signal impairments through simulations and measurements. The main goal is to evaluate the usefulness of the method for OSNR monitoring, but also to find important issues in the construction of the polarimeter and to develop necessary signal processing software. In this thesis, the main focus is 28 GBd DP-QPSK signals, as they are suggested as the standard for the 100 Gb/s networks currently being deployed [5].

This report is divided into six chapters. After the introduction, a more thorough background to fiber optical communication and OSNR measuring methods is given in Chapter 2. In Chapter 3, the Stokes-parameter-based OSNR measuring method is described in detail, including both theoretical work and the physical setup used. Chapter 4 presents the simulations performed, as well as the results obtained, and in Chapter 5 the experiments done are reported, including setups and results. Finally, the conclusions are presented in Chapter 6.

2 | Background

IN THIS CHAPTER some background to the field of optical communication and OSNR-monitoring is presented.

2.1 Optical modulation

Fiber-optical communication uses light as an electromagnetic carrier wave to transmit information through optical fibers. A general optical carrier can be described by

$$\mathbf{E}(t) = \hat{\mathbf{e}}\mathrm{Re}\left[a\exp(j\phi - j\omega_0 t)\right], \tag{2.1}$$

where $\hat{\mathbf{e}}$ is the polarization direction, a the amplitude, ϕ the phase and ω_0 the angular frequency of the carrier. All of these properties can be varied to encode information on the carrier wave, a process called modulation. The simplest modulation format, traditionally used in fiber-optic systems, is on-off keying (OOK) where the amplitude is changed between $a = 0$ (off) and $a = 1$ (on). This is the simplest form of amplitude shift keying (ASK). Also the phase ϕ can be modulated, which is called phase shift keying (PSK). A common example of a phase shift keying format is quaternary phase shift keying (QPSK) where the phase can take four different values. Another way of describing this is as a complex phasor envelope, $A = ae^{j\phi} = a(\cos\phi + j\sin\phi)$. To visualize such a signal the phasor can be plotted in the complex plane, in a constellation diagram. It is common to call the real part the in-phase component, I, and the imaginary part the quadrature component Q. In figure 2.1 constellation diagrams for OOK, QPSK and 8-PSK can be seen.

The main reason for using higher order modulation formats is to be able to encode multiple bits on each symbol and thus increasing data throughput. Other ways of increasing the throughput is to use several wavelength channels, which is called wavelength division multiplexing (WDM) or to use each wavelength to transmit two orthogonally polarized data streams. This is called polarization-division mul-

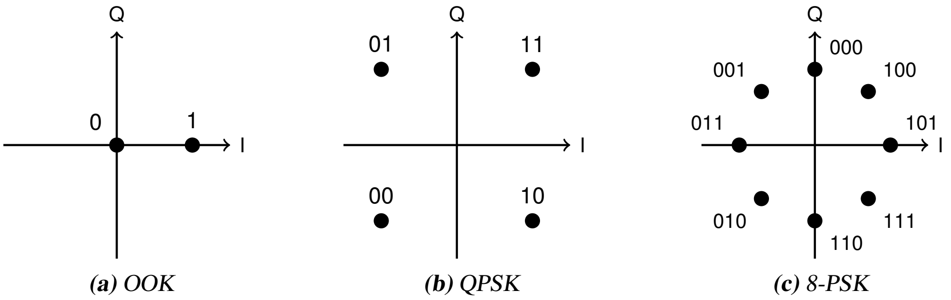

(a) *OOK* ***(b)*** *QPSK* ***(c)*** *8-PSK*

Figure 2.1: *Constellation diagrams for a few modulation formats.*

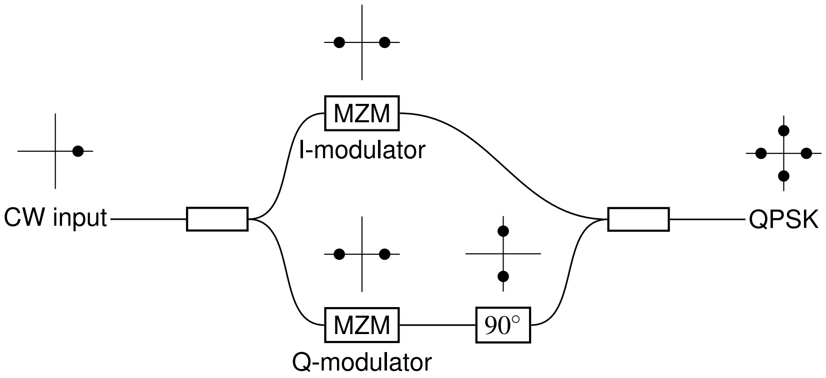

Figure 2.2: The principle of a QPSK modulator. Above the components are a small constellation diagram, to show how it changes for each step. CW stands for continuous wave and MZM for Mach-Zehnder modulator.

tiplexing, which is abbreviated PDM or PM. It can also be referred to as dual polarization (DP).

Consider the following example. Using 10 Gb/s OOK, each symbol represents one bit, a one or a zero, and the symbol rate is the same as the bit rate. If instead a DP-QPSK modulation format is used, each symbol represents four bits, since each QPSK symbol represents two bits, and two orthogonally polarized QPSK signals are transmitted. This means that the bit rate is multiplied by four, and becomes 40 Gb/s. The increase of the bit rate can of course be accomplished by using 40 Gb/s OOK, but that would also increase the bandwidth of the signal four times, which is not the case when 10 GBd DP-QPSK is used.

Of course the higher modulation formats are not without drawbacks. An OOK receiver uses the simple direct detection method, where a photodetector is used to detect the optical power. For phase modulated signals, the whole electric field needs to be detected, and a more complicated, coherent receiver is needed. However, the coherent receiver has other advantages, such as the possibility to use digital signal processing to compensate for chromatic dispersion and polarization-mode dispersion. These possibilities are due to the fact that both the amplitude and phase of the electric field can be detected.

2.1.1 A DP-QPSK modulator

Quadrature modulation can be achieved using two Mach-Zehnder modulators and a 90° phase shift. The input light is split with a 3 dB coupler, and each part is modulated with a Mach-Zehnder modulator, one for the in-phase component and one for the quadrature component. After the modulators, a 90° phase shift between the two, now modulated, parts of the signal is introduced, and they are combined again. The setup is illustrated in figure 2.2. To create a dual polarization signal, two QPSK modulators are used and their output is combined using a polarization beam combiner. Signal impairments caused by a non-ideal modulator includes quadrature error, caused by the delay not being exactly 90°, and different kinds of skew. Here skew refers to a delay between different bit-streams. For example XY-skew refers to the QPSK signals in the two polarizations are shifted in time so that the symbols in the different polarizations are not aligned in time, and IQ-skew refers to a time shift between the in-phase and quadrature components.

2.2 Optical signal-to-noise-ratio

In systems designed for transmission longer than approximately 100 km, amplification is needed to compensate for the power losses in the fiber [1]. It is obvious that this is an important topic, since many submarine and long-haul systems have a length of several thousands of kilometers. Today, in advanced WDM systems, amplification is exclusively achieved with optical amplifiers. An optical amplifier boosts the signal power in the optical domain, i.e. without needing to convert to electrical signals. This greatly reduces complexity for WDM systems. The amplifiers however give rise to noise that will degrade the signal and the bit-error-rate (BER). Therefore, the optical signal-to-noise-ratio (OSNR) is an important signal performance metric.

An important class of optical amplifiers is the erbium doped fiber amplifiers (EDFA) [1]. The EDFA is a lumped amplifier, based on stimulated emission in a gain medium, much like a laser. One of the energy transitions in erbium ions matches the standard wavelength used in long-haul fiber-optic links, 1550 nm. The amplification is achieved by exciting the erbium ions to the higher energy state of the transition. An incoming photon can then stimulate a transition from the higher to the lower state, which give rise to the emission of another photon. This photon will be an exact copy of the incoming photon, with the same wavelength, phase, propagation direction and polarization.

Apart from the stimulated emission, spontaneous electron transitions from the higher to the lower energy states also occur. The photons emitted in such a process will have random direction, polarization, phase and wavelength, within the gain band of the amplifier. The spontaneously emitted photons will then be amplified in the following amplifiers of the system, reaching the receiver as amplified spontaneous emission (ASE). The OSNR is defined as the ratio of the whole signal power and the noise power,

$$\mathrm{OSNR} = \frac{P_{\text{signal},x} + P_{\text{signal},y}}{P_{\text{noise},x} + P_{\text{noise},y}}, \tag{2.2}$$

where the noise power is measured within a specified bandwidth, usually 0.1 nm.

2.2.1 Monitoring methods

Linear interpolation methods

The conventional method for measuring OSNR uses an optical spectrum analyzer (OSA) to measure the noise power in the frequencies between the WDM channels and the signal power at the signal wavelengths [2]. The noise power at the signal wavelengths is then found by using linear interpolation. This is an example of an out of band OSNR monitoring technique. In figure 2.3 the concept is illustrated in a plot of a typical signal spectrum. It relies on the two assumptions that, firstly, the noise level can be measured between the channels, and secondly that the noise at the signal wavelength actually can be determined by interpolation. This is true for conventional point-to-point transmission systems, where the noise level is fairly uniform. However, in for example Nyquist filtered systems with a small channel spacing the first assumption is not true, i.e. the power level between the channels does not represent only the noise power, but contains a fraction of the signal power as well. The second assumption does not hold for reconfigurable systems, were different channels may have passed through a different number of EDFAs and consequently have different OSNR values [2].

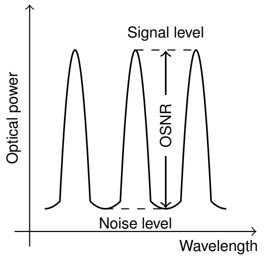

Figure 2.3: *The traditional OSNR measuring method.*

Polarization-based methods

Another class of OSNR monitoring methods proposed is based on the different polarization properties of the signal and the ASE noise. These techniques relies on the assumption that the signal contains all its power in one polarization state, while the ASE generally is unpolarized [2]. Obviously, this does not apply to polarization multiplexed signals. Polarization based techniques are generally also sensitive to polarization effects in the fiber, such as polarization mode dispersion (PMD) and polarization dependent loss (PDL). However, in [6] a method that overcomes these limitations for single polarization signals is described.

Interferometer-based methods

The interferometer methods are based on the assumption that the signal is highly coherent, while the ASE noise is incoherent. Then, the total signal can be measured by combining the two arms of a Mach-Zender delay interferometer (MZDI) constructively, and the noise power can be measured by combining them destructively. However, the assumption is not entirely valid, which introduces errors in the OSNR measurement [2].

Reference trace method

The reference trace method uses knowledge of the spectral shape of the noiseless signal to measure the noise power. The reference spectrum can be found by using a polarization resolved OSA for single polarization signals, but for dual polarization signals the reference spectrum needs to be measured at or near the transmitter [7].

2.3 Other signal impairments

In this section, signal impairments other than ASE noise are briefly described.

2.3.1 Chromatic dispersion

An important signal impairment in single mode fiber (SMF) is chromatic dispersion (CD), which causes pulse broadening because of the group velocity being wavelength dependent. This means that the spectral components of the signal propagate with different velocities. The CD in SMF is caused by two phenomena, material dispersion and waveguide dispersion. The material dispersion is caused, as the name reveals, by the dispersive properties of the fiber material, silica. The waveguide dispersion is caused by the shape of the waveguide, and can be used to tune the dispersion of the fiber.

The effects of chromatic dispersion can be described by the transfer function

$$H_f(z,\omega) = \exp\left(\frac{j\beta_2\omega^2 z}{2} + \frac{j\beta_3\omega^3 z}{6}\right), \tag{2.3}$$

where z is the length of the fiber, β_2 is the group-velocity dispersion parameter, and β_3 is the third-order dispersion parameter. The parameters β_2 and β_3 are properties of the fiber.

Chromatic dispersion is traditionally compensated for by using dispersion compensation fiber (DCF) for which β_2 has the opposite sign. In coherent systems it is common to use digital signal processing for dispersion compensation.

2.3.2 Polarization-mode dispersion

Fiber birefringence causes a phenomenon known as polarization-mode dispersion (PMD). The birefringence is caused by the fiber cross-section being slightly elliptic. This causes the group-velocity to be polarization dependent, with a fast and a slow axis. The delay between the two orthogonal polarization states is called differential group delay (DGD). As the amount and direction of the ellipticity varies randomly over the fiber length, both the amount and the axis of the DGD varies randomly.

For single polarization OOK signals the PMD causes pulse broadening, much like chromatic dispersion, but to a much lesser extent. However, for dual polarization signals, PMD can also cause crosstalk between the polarizations. This is the case when the signal polarizations are not aligned with the fast and slow axis of the birefringence. PMD effects can be compensated for with optical components [1], or with digital signal processing in coherent systems [8].

3 | The Stokes polarimeter OSNR monitor

IN THIS CHAPTER the Stokes polarimeter method for OSNR monitoring is described in detail, including both the theoretical background and practical issues.

3.1 Theoretical background

3.1.1 Polarized light and the Stokes parameters

A natural way of describing polarized light is in terms of the electric field vector **E** itself. This vector is known as the Jones vector, after the American physicist R. C. Jones [9]. The two components represent the two orthogonal, linearly polarized components of the the field,

$$\mathbf{E} = \begin{pmatrix} E_x \\ E_y \end{pmatrix} = \begin{pmatrix} E_{0x}e^{j\phi_x} \\ E_{0y}e^{j\phi_y} \end{pmatrix}, \tag{3.1}$$

here written in complex phasor form.

Another way of describing polarized light is in terms of the four Stokes parameters, that can be combined into the Stokes vector [10]. Written in terms of the Jones vector components they are

$$\mathbf{S} = \begin{pmatrix} S_0 \\ S_1 \\ S_2 \\ S_3 \end{pmatrix} = \begin{pmatrix} |E_x|^2 + |E_y|^2 \\ |E_x|^2 - |E_y|^2 \\ E_x^* E_y + E_x E_y^* \\ -jE_x^* E_y + jE_x E_y^* \end{pmatrix}, \tag{3.2}$$

where S_0 represents the total power of the light, S_1 the prevalence of 0° linear polarized light over 90° polarized light, S_2 the prevalence of 45° linear polarized light over −45° polarized light and S_3 the prevalence of right-hand circularly polarized light over left-hand.

The last three Stokes parameters form a three dimensional space, often referred to as the Stokes space. For fully polarized light the Stokes parameters are related by $S_0^2 = S_1^2 + S_2^2 + S_3^2$. The sphere formed by the Stokes parameters is called the Poincaré sphere, which is shown in figure 3.1.

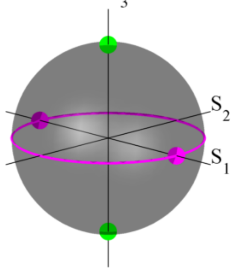

Figure 3.1: The Poincaré sphere. The dots at the poles represent circular polarization and the equator represents linear polarization.

It should be noted that the Stokes parameters usually are expressed as time averages. As all light is polarized instantaneously, this is necessary to be able to distinguish between polarized and unpolarized light. The implication of this is that what determines if light is considered polarized or unpolarized is the time of the averaging. In this work it is assumed that the time of the averaging is short enough for all light to be described as polarized. In reality the averaging time is determined by the bandwidth of the measuring device used.

For describing a modulated signal it is convenient to scale the radius of the Poincaré sphere with the average power, which differs from the common practice of using the inside of the sphere for partially polarized light [11].

3.1.2 Representation of a modulated signal

The main focus in this work is on the dual polarization QPSK modulation format, and as a start, the Stokes representation of such a signal will be derived. The symbols of a DP-QPSK signal can be described by the Jones vector

$$\mathbf{E}_{QPSK} = \frac{1}{\sqrt{2}} \begin{pmatrix} e^{j\phi_x} \\ e^{j\phi_y} \end{pmatrix}, \tag{3.3}$$

where $1/\sqrt{2}$ is included for normalization and ϕ_x and ϕ_y represent the discrete phases of the QPSK symbols. In Stokes space, this is equivalent to

$$S_1 = 0 \tag{3.4}$$

$$S_2 = \frac{e^{j(\phi_y-\phi_x)} + e^{-j(\phi_y-\phi_x)}}{2} = \cos(\phi_y - \phi_x) \tag{3.5}$$

$$S_3 = \frac{e^{j(\phi_y-\phi_x)} - e^{-j(\phi_y-\phi_x)}}{2j} = \sin(\phi_y - \phi_x), \tag{3.6}$$

where $\phi_y - \phi_x = n \cdot \pi/2$ with $n = 0, \ldots, 3$, i.e. the possible phase differences between the polarizations are multiples of $\pi/2$. Thus, the symbols of a DP-QPSK signal will result in four points in Stokes space, lying in the S_2-S_3 plane. In the case of a pure phase modulation with a constant amplitude, S_1 will always be zero, and the signal will move in the S_2-S_3 plane. However, for other kinds of transitions, the Stokes representation will be more complicated. Instead, we can find the boundaries in Stokes space for a general dual polarization complex modulation format.

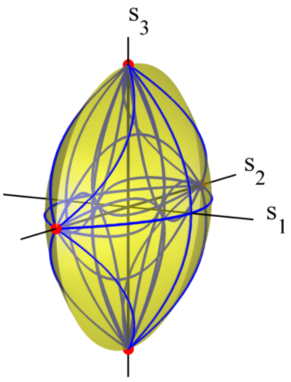

Figure 3.2: DP-QPSK in Stokes space, with the disc described in (3.8). The dots at the intersections between the disc and the S_1 and S_2 axes marks the decision points, which are degenerated in Stokes space.

Consider a complex modulation format, normalized to fit into a unit circle in the complex plane. To find the boundaries in Stokes space, choose one of the polarizations to have maximum amplitude, i.e. $E_x = 1$. Let the other polarization take any value inside the unit circle. This can be described by the Jones vector

$$\mathbf{E} = \frac{1}{\sqrt{2}} \begin{pmatrix} 1 \\ re^{j\phi} \end{pmatrix}, \tag{3.7}$$

where r is the amplitude and ϕ the phase angle. Using equation (3.2) to calculate the Stokes vector gives

$$\mathbf{S} = \frac{1}{2} \begin{pmatrix} 1+r^2 \\ 1-r^2 \\ 2r\cos\phi \\ 2r\sin\phi \end{pmatrix}. \tag{3.8}$$

In Stokes space, this describes a paraboloidal surface. Choosing the other polarization component to be 1, and letting the other vary inside the unit circle will result in another paraboloidal surface, turned in the opposite direction. Together these surfaces describe a disc or lens-like shape in Stokes space, that defines the boundaries of the signal. The disc is shown in figure 3.2.

3.1.3 Polarization of the signal

The orientation of the coordinate system used in Stokes space depends on the basis used for the polarization. To describe a signal it is convenient to align the coordinate system with the polarization of the signal by choosing the S_1 direction to be parallel with the normal of the disc.

In a measuring device, the axes are defined by the orientation of the device. Generally, the polarization of an optical signal is not stable, so if the coordinate system used is not aligned with the signal, the orientation of the disc will fluctuate with the polarization of the signal. In the previous description it assumed that the polarization of the signal is stable.

3.1.4 Noise in Stokes space

The ASE noise in an optical system can be described with the Jones vector

$$\mathbf{n} = \begin{pmatrix} n_x \\ n_y \end{pmatrix}, \tag{3.9}$$

where n_x and n_y are complex Gaussian random variables with the same variance, i.e. $\mathrm{Var}(n_x) = \mathrm{Var}(n_y) = \mathrm{Var}(n)$. The ASE noise consists of photons with random polarization, which means that when the time averaged Stokes parameters are used, the noise is unpolarized. However, if a short averaging time is used, the noise has some random polarization and will form a sphere in Stokes space.

To measure the OSNR we must find a way to measure the noise power separated from the signal power and a measure of the signal power. If we consider the noisy signal

$$\mathbf{E}_n = \begin{pmatrix} E_x + n_x \\ E_y + n_y \end{pmatrix}, \tag{3.10}$$

the corresponding Stokes parameters will be a mix of the signal and noise Stokes parameters. Inserting $\mathbf{E}_n$ into (3.2), we obtain

$$S_1 = |E_x|^2 - |E_y|^2 + |n_x|^2 - |n_y|^2 + E_x n_x^* + E_x^* n_x - E_y n_y^* - E_y^* n_y, \tag{3.11}$$

$$S_2 = E_x E_y^* + E_x^* E_y + n_x n_y^* + n_x^* n_y + E_x n_y^* + E_x^* n_y + E_y n_x^* + E_y^* n_x, \tag{3.12}$$

$$S_3 = E_x E_y^* - E_x^* E_y + n_x n_y^* - n_x^* n_y + E_x n_y^* - E_x^* n_y + E_y n_x^* - E_y^* n_x. \tag{3.13}$$

It is not obvious from these expressions if any of the Stokes parameters of a noisy signal can be used as a measure of the noise power, but the thickness of the disc is less dependent on the signal power than the diameter. To illustrate this, the distance from the S_1 axis, i.e. $\sqrt{S_2^2 + S_3^2}$ and the distance from the S_2-S_3 plane, i.e. $|S_1|$ is plotted in figure 3.3. Therefore, the ratio between the diameter and the thickness of the disc is a good candidate for the OSNR measure.

As a measure of thickness of the lens we can use $\mathrm{Var}(S_1)$ and as a measure of the radius we can use $(\mathrm{Var}(S_2) + \mathrm{Var}(S_3))/2$. Using equation (3.11) we have

$$\mathrm{Var}(S_1) = \mathrm{Var}(|E_x|^2 - |E_y|^2) + \mathrm{Var}(n)(\mathrm{Var}(\mathrm{Re}[E_x]) + \mathrm{Var}(\mathrm{Re}[E_y])) + 2\mathrm{Var}^2(n)$$

$$\mathrm{Var}(S_2) = \mathrm{Var}(E_x E_y^* + E_x^* E_y) + \mathrm{Var}(n)(\mathrm{Var}(\mathrm{Re}[E_x]) + \mathrm{Var}(\mathrm{Re}[E_y])) + 2\mathrm{Var}^2(n)$$

$$\mathrm{Var}(S_3) = \mathrm{Var}(E_x E_y^* - E_x^* E_y) + \mathrm{Var}(n)(\mathrm{Var}(\mathrm{Im}[E_x]) + \mathrm{Var}(\mathrm{Im}[E_y])) + 2\mathrm{Var}^2(n).$$

If E_x and E_y are uncorrelated and have zero mean, which is safe to assume in real systems, we can use the following property of the variance [12]

$$\mathrm{Var}(X - Y) = \mathrm{Var}(X) + \mathrm{Var}(Y) \tag{3.14}$$

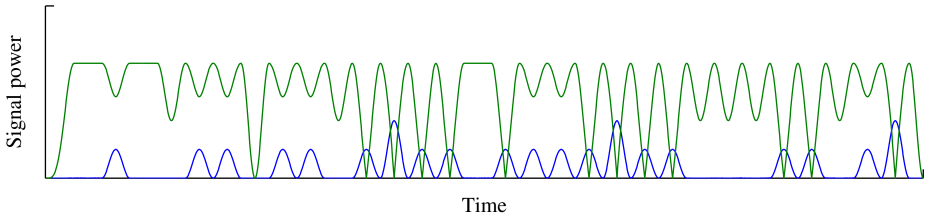

Figure 3.3: The upper line is the distance from the S_1 axis, i.e. $\sqrt{S_2^2+S_3^2}$ and the lower line is the distance from the S_2-S_3 plane, i.e. $|S_1|$, vs. time. The plot illustrates the greater impact of the signal power on the radius of the disc than on the thickness for DP-QPSK.

to find that:

$$\mathrm{Var}\left(|E_x|^2-|E_y|^2\right)=\mathrm{Var}\left(|E_x|^2\right)+\mathrm{Var}\left(|E_y|^2\right)\propto \mathrm{Var}\left(S\right)\propto S^2 \tag{3.15}$$

and

$$\mathrm{Var}\left(E_xE_y^*+E_x^*E_y\right)=\mathrm{Var}\left(\mathrm{Re}\left[E_xE_y\right]\right)\propto \mathrm{Var}\left(S\right)\propto S^2, \tag{3.16}$$

where S is the total signal power.

Now we can that the first, quadratic terms are proportional to the signal power S squared, the second terms are proportional to the signal power times the noise power N and the third terms are proportional to the noise power squared. This yields

$$\mathrm{Var}\left(S_1\right)\propto k_{21}S^2+k_1SN+k_0N^2, \tag{3.17}$$

$$\mathrm{Var}\left(S_2\right)\propto k_{22}S^2+k_1SN+k_0N^2. \tag{3.18}$$

Now it is time to introduce $OSNR\propto S/N$,

$$\mathrm{Var}\left(S_1\right)\propto k_{21}N^2OSNR^2+k_1N^2OSNR+k_0N^2 \tag{3.19}$$

$$\mathrm{Var}\left(S_2\right)\propto k_{22}N^2OSNR^2+k_1N^2OSNR+k_0N^2. \tag{3.20}$$

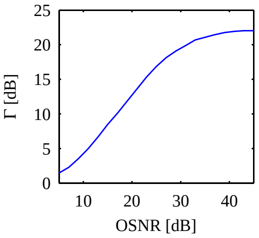

Figure 3.4: A typical simulated Γ vs. OSNR curve.

It follows that the thickness-radius ratio

$$\Gamma=\frac{\mathrm{Var}\left(S_2\right)+\mathrm{Var}\left(S_3\right)}{2\mathrm{Var}\left(S_1\right)}=\frac{k_{22}OSNR^2+k_1OSNR+k_0}{k_{21}OSNR^2+k_1OSNR+k_0}, \tag{3.21}$$

is a function of the OSNR. The usefulness of Γ as a measure of the OSNR is determined by the values of the constants. In figure 3.4, a Γ vs. OSNR curve for a DP-QPSK signal is plotted.

In the case of no signal, with $OSNR=0$, $\Gamma=k_0/k_0=1$. This means that only noise is present, which is represented by a sphere in Stokes space. When there is no noise present,

$$OSNR\to\infty \quad\Rightarrow\quad \Gamma\to\frac{k_{22}}{k_{21}}. \tag{3.22}$$

This means that Γ has a maximum value, which sets a limit for how high values of OSNR that can be measured. The actual usable limit is lower, as a small change in Γ requires a large change in OSNR.

By assuming that k_0 is negligible, Eq. (3.21) can be approximated by

$$\Gamma\approx\frac{k_{22}OSNR+k_1}{k_{21}OSNR+k_1}=\frac{k_{22}}{k_{21}OSNR+k_1}OSNR+\frac{k_1}{k_{21}+k_1}. \tag{3.23}$$

For OSNR-values where $k_{21}OSNR\ll k_1$ this is simplified further to the linear approximate relation

$$\Gamma\approx\frac{k_{22}}{k_1}OSNR+\frac{k_{21}}{k_1}, \tag{3.24}$$

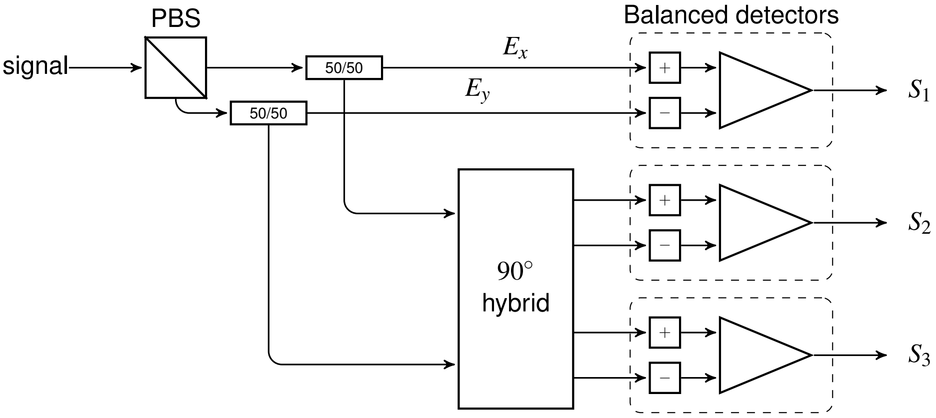

Figure 3.5: *The polarimeter setup.*

which can be seen as the linear part of the curve in figure 3.4. In the linear part, the slope is approximately k_{22}/k_1.

To estimate the OSNR from Γ the inverse of Eq. (3.21) is needed. By solving Eq. (3.21) for OSNR it is found to be

$$OSNR(\Gamma) = \frac{-k_1(1-\Gamma)+\sqrt{k_1^2(1-\Gamma)^2 - 4k_0(k_{22}-k_{21}\Gamma)(1-\Gamma)}}{2(k_{22}-k_{21}\Gamma)}. \tag{3.25}$$

3.2 Implementation and practical issues

The Stokes parameters can be directly measured with several set-ups. The method used in this work makes use of a polarization beam splitter (PBS) and a 90° hybrid similar to that in a coherent receiver. In a practical implementation a number of issues have to be addressed, both relating to the nature of the signal and to the imperfections of the components used.

3.2.1 Principle of operation

The hybrid-based polarimeter setup uses a PBS to split the signal into orthogonal polarization states. To extract S_1, the two branches are fed directly into the ports of a balanced detector. To extract S_2 and S_3, two 3 dB couplers are used to feed the two branches into a 90° hybrid. Figure 3.5 shows the setup.

In figure 3.6a the details of the 90° hybrid can be seen. The equations for the outputs are

$$E_1 = \frac{1}{2}(E_x + E_y), \tag{3.26}$$

$$E_2 = \frac{1}{2}(E_x - E_y), \tag{3.27}$$

$$E_3 = \frac{1}{2}(E_x + jE_y), \tag{3.28}$$

$$E_4 = \frac{1}{2}(E_x - jE_y), \tag{3.29}$$

where the factor $1/2$ is caused by the the power splitting and corresponds to a power splitting of $(1/2)^2 = 1/4$. The actual outputs are also multiplied by a con-

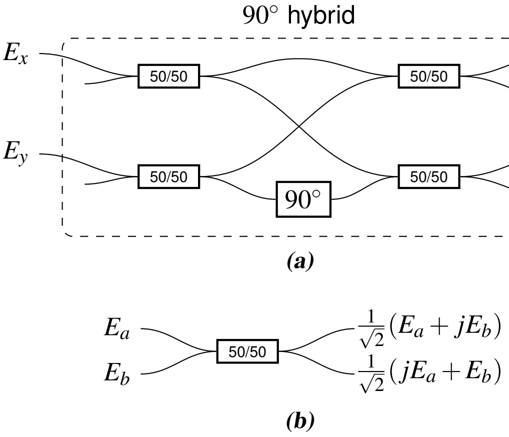

Figure 3.6: *Details of the hybrid and the 3 dB coupler. (a) A schematic view of the 90° hybrid. (b) Equations for input and output fields from a 3 dB coupler.*

stant phase. The Stokes parameters S_2 and S_3 can be extracted by

$$S_2 = 4(|E_1|^2 - |E_2|^2) \tag{3.30}$$

$$S_3 = 4(|E_3|^2 - |E_4|^2), \tag{3.31}$$

which is easily accomplished with balanced detectors.

3.2.2 Hybrid imperfections

The optical 90° hybrid is an important component of the polarimeter, and even small imperfections will affect the results to a significant degree. However, as will be shown in the following section, the most important impairments can be compensated for with signal processing.

The hybrid imperfections considered here are losses and errors to the 90° angle. This is done by introducing loss coefficients and replacing j with $e^{j\phi}$, where the angle $\phi \approx \pi/2$. Equation (3.26) is now modified to:

$$E_1 = k_{x1}E_x + k_{y1}E_y \tag{3.32}$$

$$E_2 = k_{x2}E_x - k_{y2}E_y \tag{3.33}$$

$$E_3 = k_{x3}E_x + k_{y3}e^{j\phi}E_y \tag{3.34}$$

$$E_4 = k_{x4}E_x - k_{y4}e^{j\phi}E_y, \tag{3.35}$$

and the measured Stokes parameters are

$$S'_2 = (k_{x1}^2 - k_{x2}^2)|E_x|^2 + (k_{y1}^2 - k_{y2}^2)|E_y|^2 + (k_{x1}k_{y1} + k_{x2}k_{y2})S_2 \tag{3.36}$$

$$S'_3 = (k_{x3}^2 - k_{x4}^2)|E_x|^2 + (k_{y3}^2 - k_{y4}^2)|E_y|^2 + (k_{x3}k_{y3} + k_{x4}k_{y4})(S_2 \cos\phi - S_3 \sin\phi). \tag{3.37}$$

Losses outside of the hybrid (for example different losses for E_x and E_y or detector imbalance) can be included in these expressions as well. Note that even for an ideal hybrid, all coefficients will be $\frac{1}{2}$ because of the power splitting. For an ideal hybrid, $\phi = 90°$. Inserting this into the above equations yields

$$S'_2 = \frac{1}{4}S_2 \tag{3.38}$$

$$S'_3 = \frac{1}{4}S_3, \tag{3.39}$$

which is consistent with equation 3.30.

Another observation that can be made is that as long as the loss coefficients are equal, the only effect the imperfections will have is a scaling. The expressions can be simplified further by observing that any linear combination of $|E_x|^2$ and $|E_y|^2$ can be written in terms of S_0 and S_1, i.e. $|E_x|^2 = \frac{1}{2}(S_0 + S_1)$ and $|E_y|^2 = \frac{1}{2}(S_0 - S_1)$. To investigate the effect of the imperfections further, it is convenient to introduce new coefficients and write

$$S_2' = \ell_{20}S_0 + \ell_{21}S_1 + \ell_{22}S_2, \tag{3.40}$$

$$S_3' = \ell_{30}S_0 + \ell_{31}S_1 + \ell_{32}S_2 + \ell_{33}S_3. \tag{3.41}$$

If we include losses in the different polarization branches also S_1 is affected

$$S_1' = \ell_{10}S_0 + \ell_{11}S_1. \tag{3.42}$$

This can be written in form of a matrix multiplication

$$\mathbf{S}' = \begin{pmatrix} S_0' \\ S_1' \\ S_2' \\ S_3' \end{pmatrix} = \begin{pmatrix} \ell_{00} & 0 & 0 & 0 \\ \ell_{10} & \ell_{11} & 0 & 0 \\ \ell_{20} & \ell_{21} & \ell_{22} & 0 \\ \ell_{30} & \ell_{31} & \ell_{32} & \ell_{33} \end{pmatrix} \begin{pmatrix} S_0 \\ S_1 \\ S_2 \\ S_3 \end{pmatrix} = \mathbf{LS}. \tag{3.43}$$

If the simplification is made that S_0 is constant, its influence can be removed by a DC-block. If the numerical values of the imperfections are known, the actual Stokes parameters can be found by solving (3.43), and the actual Stokes parameters are given by

$$\mathbf{S} = \mathbf{L}^{-1}\mathbf{S}'. \tag{3.44}$$

3.2.3 Tracking of polarization state and phase differences

As mentioned previously, polarization fluctuations of the signal will cause the disc to rotate in the coordinate system of the polarimeter. In addition to the rotation due to polarization fluctuations, further rotations are caused by phase fluctuations in the two arms of the polarimeter, after the PBS. Phase differences between the inputs of the hybrid will cause a rotation of the disc around the S_1-axis (in the measurement system).

This can be understood by considering 45° linearly polarized CW light, that will be represented by a point on the intersection of the positive S_2 axis and the Poincaré sphere. A phase shift between the x and y components will transform the linearly polarized light to elliptical or even circular polarized light, moving the point along a circle in the S_2-S_3 plane. For a modulated signal, this will cause a rotation of the disc around the S_1-axis.

Acting together, these rotations causes the orientation of the disc to fluctuate in all directions, and to measure the dimensions of the disc, these need to be tracked. This can be done by using a simple plane fitting algorithm, such as the singular value decomposition (SVD). In fact, the three singular values correspond directly to the dimensions of the disc.

The SVD is a factorization of an $m \times n$ matrix [13, 14]

$$\mathbf{A} = \mathbf{U}\Sigma\mathbf{V}^*, \tag{3.45}$$

where **U** is an $m \times m$ matrix, Σ is an $m \times n$ diagonal matrix and **V** is an $n \times n$ matrix. To use it for plane fitting, set **A** to be the coordinates of a set of 3D points

$$\mathbf{A} = \begin{pmatrix} p_{1x} & p_{1y} & p_{1z} \\ \vdots & \vdots & \vdots \\ p_{mx} & p_{my} & p_{mz} \end{pmatrix}. \tag{3.46}$$

The columns of **V** will form a basis, oriented with the axes of the ellipsoid closest to the set of points in **A**. Figure 3.7 shows an ellipsoid together with the basis formed by its semi-axes. In particular, the third column will be the normal to the closest plane. Now, the problem could be solved by doing a coordinate transformation to the basis found by the SVD and then calculating the dimensions of the disc according to equation (3.21). However, the SVD provides us also with this information. The diagonal of the middle matrix in the decomposition, Σ, contains the singular values of **A**

$$\Sigma = \begin{pmatrix} \sigma_1 & 0 & 0 \\ 0 & \sigma_2 & 0 \\ 0 & 0 & \sigma_3 \\ 0 & 0 & 0 \\ & \vdots & \\ 0 & 0 & 0 \end{pmatrix}. \tag{3.47}$$

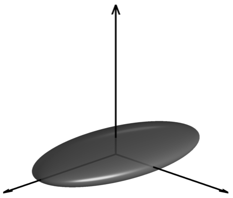

Figure 3.7: *An ellipsoid together with the basis formed by its semi-axes.*

Here, σ_1, σ_2 and σ_3 correspond to the semi-axes of the ellipsoid closest to the point set. The square sum of the distances from the points to the best fitted plane is σ_3^2, and the square sum of the distances between the points and the normal to the closest plane is $\sigma_1^2 + \sigma_2^2$ [13]. This means that if the point set are measurements of the signal in Stokes space, σ_1, σ_2 and σ_3 are equal to $\mathrm{Var}(S_1)$, $\mathrm{Var}(S_2)$ and $\mathrm{Var}(S_3)$ respectively, and the ratio between the diameter and the thickness of the disc is:

$$\Gamma = \frac{\sigma_2^2 + \sigma_3^2}{2\sigma_1^2}. \tag{3.48}$$

The columns of **V** define the coordinate system in Stokes space of the signal, with the third column corresponding to the S_1 direction.

4 | Simulations

COMPUTER SIMULATIONS have been carried out both to study the effect of different signal impairments on the Stokes space representation of the signal, and to study the behavior of the whole system without the constraints of available equipment. The simulations were also used to find the cause of different problems encountered during the experimental work. In this chapter the methods used are described, and the main results are presented and discussed.

4.1 Method

4.1.1 Signal model

For the simulations, the Jones notation was used. For all simulations a 28 GBd DP-QPSK baseband signal was used, both Nyqvist modulated and with a raised cosine envelope.

The raised cosine pulse is described by

$$y(t) = \begin{cases} 1, & \text{if} \quad |t| < \frac{1-a}{2T} \\ \frac{1}{2}\left(1 + \cos\left(\frac{\pi}{2Ta}\left|t - \frac{1-a}{2T}\right|\right)\right), & \text{if} \quad \frac{1-a}{2T} < |t| < \frac{1+a}{2T} \\ 0, & \text{else} \end{cases}, \tag{4.1}$$

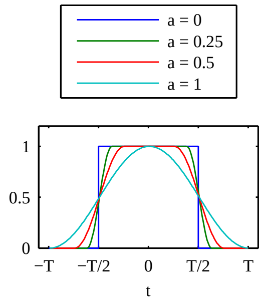

Figure 4.1: *The raised cosine pulse.*

where T is the symbol time and a is a parameter that determines the rise time of the transitions. If $a = 0$, the pulse will have a square shape and $a = 1$ gives a pulse shaped like one period of a cosine function. The raised cosine pulse can be seen in figure 4.1.

Nyqvist modulated data has a narrow rectangular-shaped spectrum, which allows extremely dense wavelength division multiplexing. This gives the pulses the shape of a sinc function in time domain

$$y(t) = \frac{\sin \pi t}{\pi t}. \tag{4.2}$$

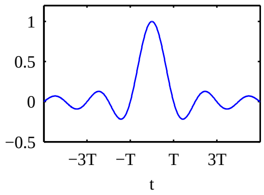

Figure 4.2: *The sinc-pulse. Note that the timescale is different from 4.1.*

The sinc-pulse can be seen in figure 4.2.

The data used was a pseudorandom binary sequence (PRBS), that was circularly shifted for the different quadrature components. Figure 4.3 shows the parts of the simulated transmitter.

4.1.2 ASE model

The ASE noise was modeled in the frequency domain as spectrally flat noise with random phase. This was implemented by adding

$$E_{noise} = ne^{j\phi_{rand}}, \tag{4.3}$$

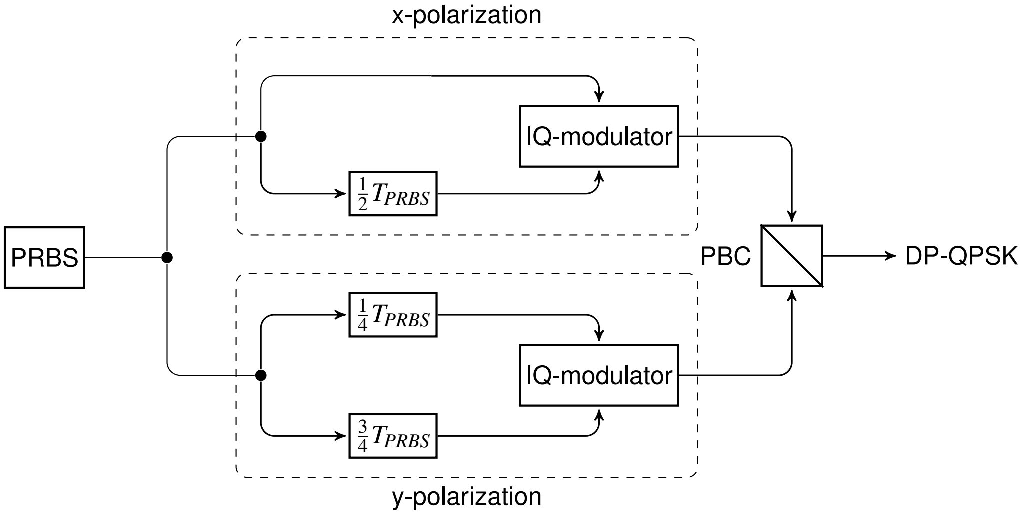

Figure 4.3: *The simulated transmitter setup. The same PRBS is used for I_x, I_y, Q_x and Q_y, but delayed a fraction of the PRBS word length.*

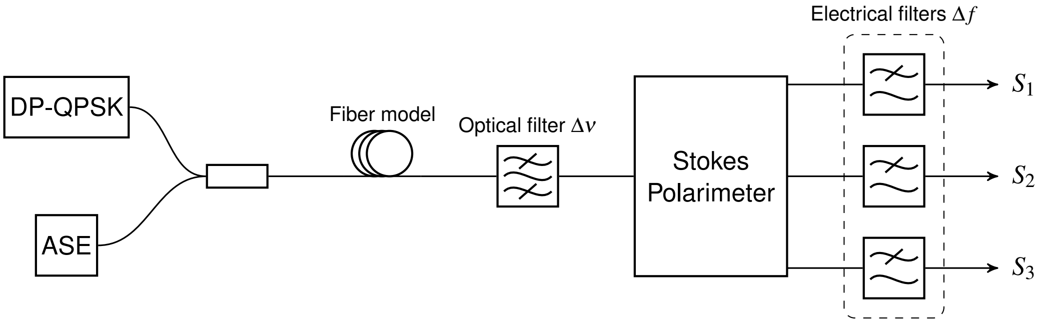

Figure 4.4: *The simulated system setup.*

at each sample point of the signal in the frequency domain. Here n is a constant and $\phi_{rand} \sim U(0, 2\pi)$ is a random variable uniformly distributed between 0 and 2π.

4.2 Results

Generally, the simulation results are presented either in the form of a Γ vs OSNR curve or as a plot of the maximum Γ value, i.e. Γ for a noiseless signal vs. the parameter of interest. The Γ vs. OSNR curve is typically fairly linear for low OSNR values, but starts to saturate for higher values and reaches a maximum value. As the curve becomes less steep the uncertainty of the OSNR estimate becomes higher, so the maximum Γ value essentially determines the maximum OSNR value that is possible to measure. Therefore it is desirable with a steep slope and a high maximum Γ.

It is also desirable that the behavior does not change when parameters outside the polarimeter setup changes, for example different pulse shapes and signal impairments. Thus, the Γ value for a noise free signal gives an indication of how well the method behaves.

4.2.1 Bandwidths and pulse shapes

The signal is filtered in two places in the setup. The first is the optical filter, whose main purpose is to select the channel to be measured upon, and the second place is after the polarimeter, were the signal is transferred to the electrical domain. The optical bandwidth $\Delta\nu$ of the filter, must be narrow enough to suppress the neighboring channels and wide enough to let a sufficient amount of the signal through. It is not obvious what effect different values of the optical bandwidth have, and this was investigated with the simulations. The electrical bandwidth Δf is determined by the bandwidth of the detectors and the ADC.

Closely related to the optical bandwidth is the pulse shape, which determines the shape of the signal spectrum. To investigate the filter bandwidths separately, a square pulse was used.

Only one channel was simulated, so the effects of neighboring channels were not investigated. Also, there was a practical limit on how low electrical bandwidths could be simulated, set by the word length of the PRBS. The PRBS has a spectrum consisting of equally spaced frequency components with the spacing

$$\Delta f_{PRBS} = \frac{R_{symbol}}{2^m - 1}, \tag{4.4}$$

where R_{symbol} is the symbol rate and m is the order of the PRBS. If the spacing is to big, i.e. the word length is to short, too few of the frequency components are let through the filter and the PRBS is no longer a good model of a real signal. The problem can be solved by either using a longer word length, or by taking the average of several simulations using random data. However, both methods require more computing power, essentially setting the limit for what is reasonable to simulate. The longest PRBS possible to use with respect to simulation time was PRBS15, which is $2^{15} - 1 = 32767$ bits long. This made the lowest usable electrical bandwidth $\Delta f = 100\,\mathrm{MHz}$. In figure 4.5 the lowpass filtered signal representation in Stokes space is shown.

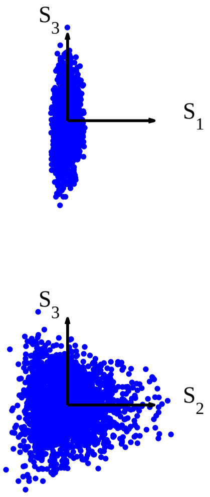

Figure 4.5: *Example of a simulated, lowpass filtered signal representation in Stokes space.*

Raised cosine pulses

In figure 4.6a-4.6d the Γ vs. OSNR curve for different bandwidth combinations can be seen. There is a clear dependence between the maximum value of Γ and the optical bandwidth, as can be seen in figure 4.6a, as well as the rise-time of the raised cosine envelope, as seen in 4.6b. Essentially, narrowing the optical bandwidth of a square-pulse signal will result in slower transitions, which explains the similarity between the optical bandwidth and the pulse shape factor. From this we can draw the conclusion that faster transitions gives a higher maximum Γ value.

This can be explained by studying for what parts of the signal S_1 is nonzero. From chapter 3 we know that the thickness of the disc for a noiseless signal only takes a non-zero value in the transitions. This means that if the signal stays in the constellations points during a larger part of the time, and less in the transitions, the influence of the signal power on the thickness of the disc will be lower. The effect of this is that the thickness will be a good measure of the noise level, also for low noise levels.

On the other hand, if the electrical bandwidth is increased the maximum Γ decreases. This can be seen by comparing figure 4.6c and 4.6d. This is consistent with the previous discussion about the optical bandwidth, as a lower electrical bandwidth will suppress the fast spikes in S_1 caused by the transitions.

From a practical point of view, the results indicate that a low electric bandwidth does not limit the usability of the method. In fact it is even desirable, both from a

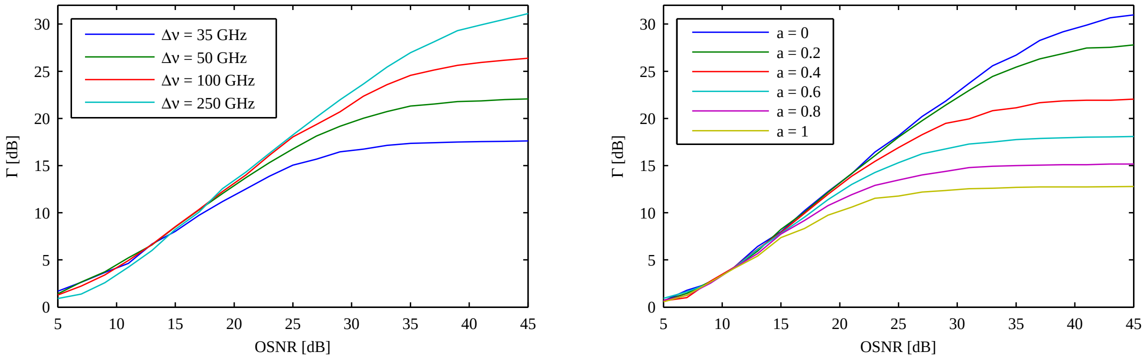

(a) *Square pulses and different optical bandwidths.* $\Delta f = 1\,GHz$ **(b)** $\Delta\nu = 250\,\mathrm{GHz}$, $\Delta f = 1\,GHz$

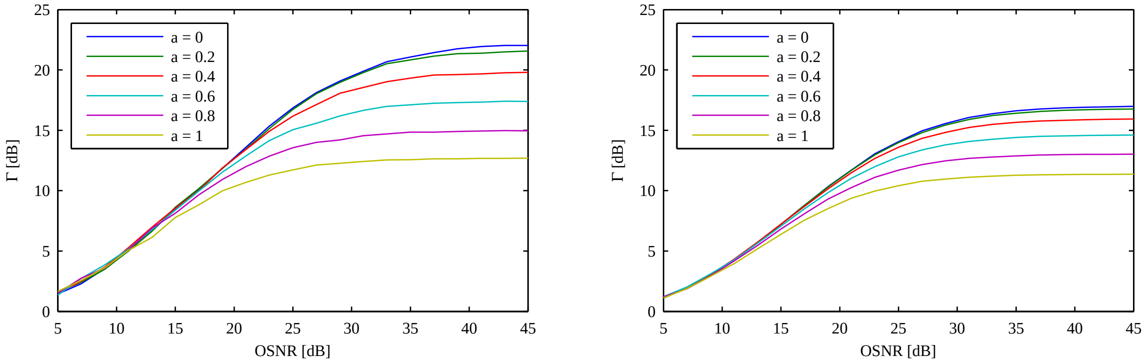

(c) $\Delta\nu = 50\,\mathrm{GHz}$, $\Delta f = 1\,\mathrm{GHz}$ ***(d)*** $\Delta\nu = 50\,\mathrm{GHz}$, $\Delta f = 20\,\mathrm{GHz}$

Figure 4.6: Γ *vs OSNR for different pulse shapes and bandwidth combinations. Figure (a) and (b) illustrate the connection between optical bandwidth and pulse shape, and that faster transitions gives a higher maximum* Γ*. Figure (c) and (d) illustrate that a higher electrical bandwidth lowers the maximum* Γ*.*

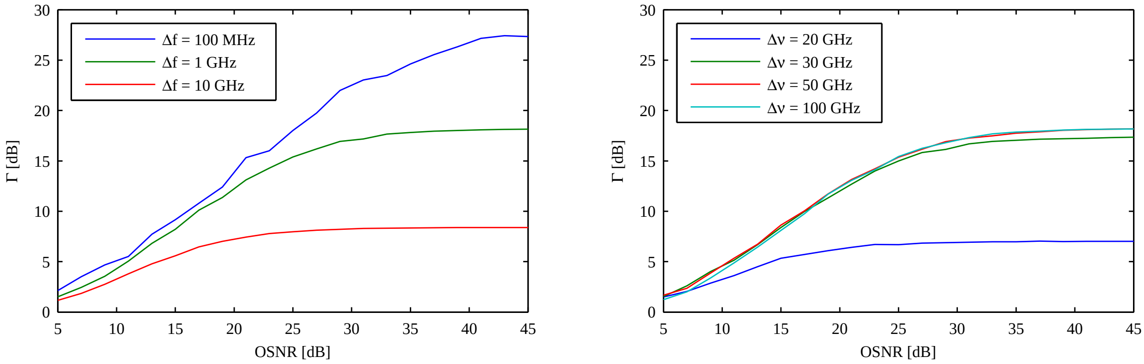

(a) $\Delta\nu = 50\,\mathrm{GHz}$ ***(b)*** $\Delta f = 1\,\mathrm{GHz}$

Figure 4.7: Γ *vs. OSNR for Nyqvist modulated data, for (a) different electrical bandwidths and (b) different optical bandwidths. The result is not affected if the optical bandwidth is not narrower than the signal bandwidth, but is sensitive to the electrical bandwidth.*

performance point of view and from an economical point of view. For the optical bandwidth, although a wider bandwidth gives a higher maximum Γ for signals with fast transitions, this also makes the method sensitive to the pulse shape of the signal. In a real system, the optical bandwidth is also limited by the channel spacing, typically 50 GHz. A good choice of optical filter would be the same shape and bandwidth as that used in the wavelength multiplexer.

Nyqvist modulated data

In figure 4.7a and 4.7b the Γ vs. OSNR curves using Nyqvist modulated data can be seen. As long as the optical bandwidth is wider than the signal bandwidth, changes in the optical bandwidth have small effect on the results. The electric bandwidth on the other hand is important, and a more narrow electric bandwidth increases the maximum Γ value significantly.

The insensitivity to the optical bandwidth is easily explained by the narrow shape of the signal spectrum for Nyqvist modulated data, but the dependence on the electric bandwidth is not as obvious. Due to the more complicated nature of the Nyqvist modulated signal it is hard to make the same kind of reasoning about the transitions as for the raised cosine pulses. The most important conclusion to draw from these results is that the OSNR dependence of Γ is also dependent on the pulse shape and signal spectrum.

4.2.2 Chromatic dispersion

The chromatic dispersion (CD) was added in the frequency domain, modeling the fiber with the transfer function

$$H_f(z,\omega) = \exp\left(\frac{j\beta_2\omega^2 z}{2} + \frac{j\beta_3\omega^3 z}{6}\right), \tag{4.5}$$

where z is the length of the fiber. β_2 and β_3 are related to the more commonly used dispersion parameter D and the dispersion slope S according to

$$\beta_2 = \frac{-\lambda^2}{2\pi c}D \quad \text{and} \quad \beta_3 = \left(S - \frac{4\pi c}{\lambda^3}\beta_2\right)\left(\frac{\lambda^2}{2\pi c}\right)^2. \tag{4.6}$$

The values used were the typical ones for standard single mode fiber (SMF), $D = 16\,\text{ps/nm/km}$ and $S = 0.09\,\text{ps/nm}^2\text{/km}$ [1].

The CD did affect the measurements, but could be compensated for easily by using a more narrow electrical bandwidth. This is demonstrated in figure 4.8, where the results for different fiber lengths are shown for different electrical bandwidths. The spectra of the Stokes parameters of the signal, plotted in figure 4.9, gives a clue to the effect of the narrower bandwidth. In figure 4.9a the spectrum for a signal without dispersion is plotted. The distance between the two curves corresponds directly to the ratio Γ. In figure 4.9b and 4.9c the signal is affected by different amounts of CD, and for high frequencies the S_1 curve is raised to the same level as the S_2 curve. This means that the ratio Γ is decreased. However, if the Stokes parameters are low-pass filtered with sufficiently low bandwidth, the bump in the S_1 curve is suppressed and Γ is unchanged.

Due to the limitations of the simulation method used, discussed in section 4.2.1, lower bandwidths than 100 MHz could not be simulated. However, the results for higher bandwidths as well as the spectral simulations gives a strong indication that large amounts of chromatic dispersion can be tolerated, given that a sufficiently low electric bandwidth is used. For example, by comparing figure 4.8a and 4.8b we can see that lowering Δf a factor of ten increases the maximum Γ for the $L = 100\,\text{km}$ curve from 10 dB to almost 20 dB. Given the results in figure 4.9, a system with $\Delta f = 10\,\text{MHz}$ will tolerate a fiber length of at least 1000 km.

4.2.3 Polarization mode dispersion

Polarization mode dispersion (PMD) to the first order can be modeled as single element of differential group delay (DGD). This is expressed as a matrix multipli-

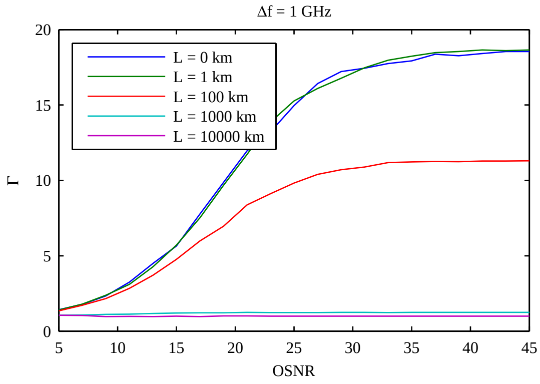

(a) $\Delta f = 1\,\text{GHz}$ ***(b)*** $\Delta f = 100\,\text{MHz}$

Figure 4.8: *Γ vs OSNR for different lengths of SMF with $D = 16\,\text{ps/nm/km}$. Note that the effect of the dispersion is negligible for $L = 100\,\text{km}$ and $\Delta f = 100\,\text{MHz}$, which was severely degraded for $\Delta f = 1\,\text{GHz}$.*

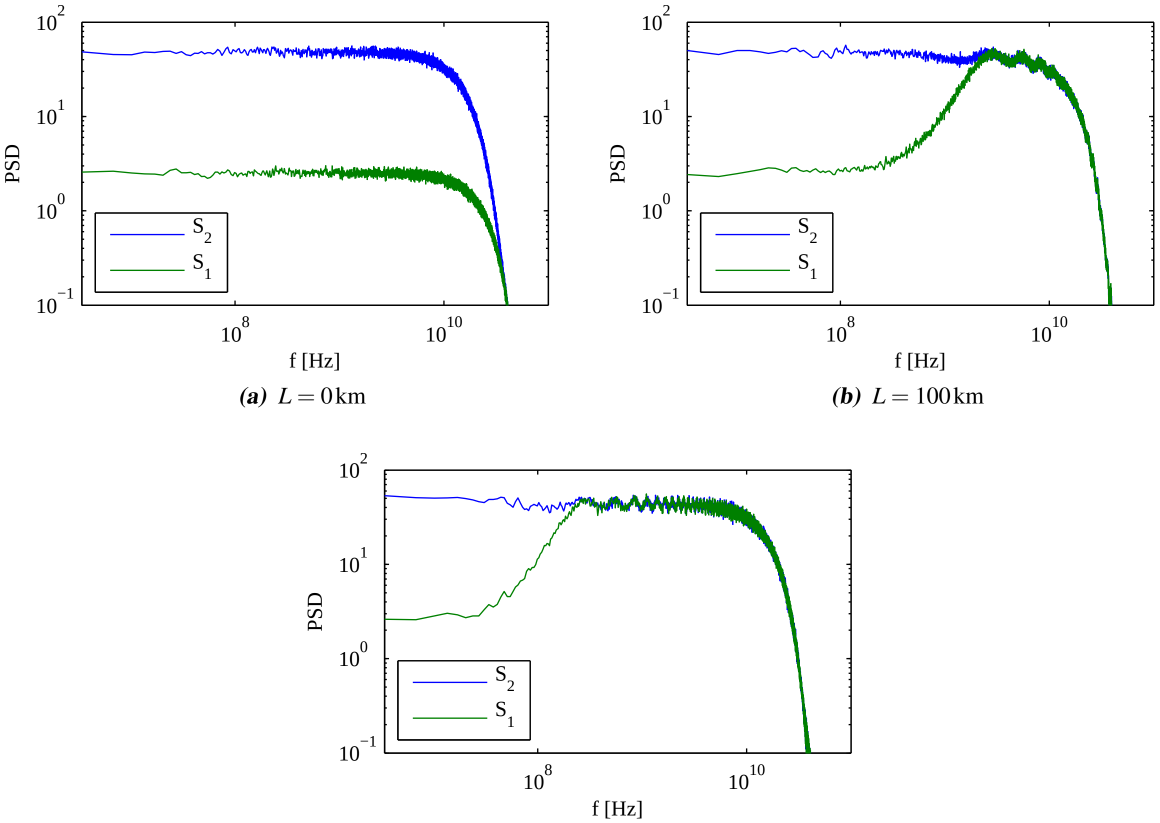

(a) $L = 0\,\text{km}$ ***(b)*** $L = 100\,\text{km}$

(c) $L = 1000\,\text{km}$

Figure 4.9: *The power spectral density of S_1 and S_2 for different lengths of SMF ($D = 16\,\text{ps/nm/km}$). The dispersion affects only the higher frequencies.*

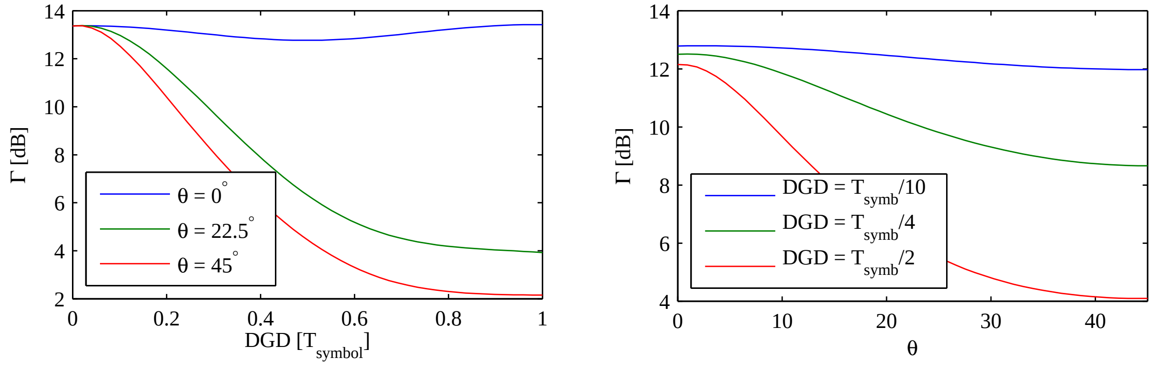

(a) ***(b)***

Figure 4.10: *The maximum* Γ *value, i.e. for a signal without noise, plotted vs the differential group delay* Δt *and the angle between the signal and the PMD axis,* θ*.*

cation in the frequency domain

$$\hat{\mathbf{E}}_{out}(\omega) = \begin{pmatrix} \exp(j\omega\Delta t/2) & 0 \\ 0 & \exp(-j\omega\Delta t/2) \end{pmatrix} \hat{\mathbf{E}}_{in}(\omega). \tag{4.7}$$

where Δt is the amount of DGD. The PMD is also characterized by the direction of the slow and fast axis of the birefringence related to the x and y polarization axes of the signal. This will be referred to as the angle θ between the signal and the DGD element. In Eq. (4.7), $\theta = 0$, and the signal is aligned with the DGD element. The angle can be changed by rotating the polarization before applying the DGD matrix. This can be done by multiplying with a rotation matrix

$$\hat{\mathbf{E}}_{out}(\omega) = \begin{pmatrix} \cos\theta & \sin\theta \\ -\sin\theta & \cos\theta \end{pmatrix} \begin{pmatrix} \exp(j\omega\Delta t/2) & 0 \\ 0 & \exp(-j\omega\Delta t/2) \end{pmatrix} \begin{pmatrix} \cos\theta & -\sin\theta \\ \sin\theta & \cos\theta \end{pmatrix} \hat{\mathbf{E}}_{in}(\omega). \tag{4.8}$$

Here, the polarization is rotated back to the original coordinate system after the DGD is applied.

Since the Stokes representation of the signal is not affected if the x and y polarizations are interchanged or if the sign of θ is changed, the effect of the PMD will symmetric around $\theta = 0^\circ$ and $\theta = 45^\circ$. This means that only values of θ in the range 0° to 45° are relevant.

As can be seen in figure 4.10 the effect of PMD on the maximum Γ value is large when the angle between the signal polarization and the PMD axis is large. Even for moderate values of DGD, the value of Γ is lowered several dB. Note that the timescale in the plot is one symbol slot, T_{symbol}, which is 35.7 ps for a 28 GBd signal.

However, for PMD aligned with the signal polarization the effect is not significant. In this case, the PMD is equivalent to a timing skew between the x- and y-polarization of the signal.

To further illustrate the effect of PMD, the Stokes representation of the signal for different DGDs and angles are plotted in figure 4.11. Here we can note that for the case were the signal polarization and the PMD axis are aligned, the Stokes representation keeps within the disc-shaped boundaries. For the worst case with the angle $\theta = 45^\circ$, the disc is totally deformed.

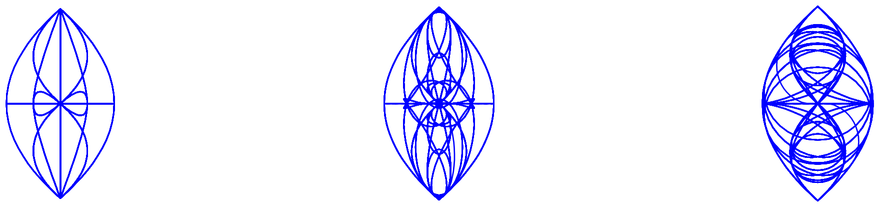

(a) *$\theta = 0^\circ$, $\Delta t = 0$* ***(b)*** *$\theta = 0^\circ$, $\Delta t = 5\,\mathrm{ps}$* ***(c)*** *$\theta = 0^\circ$, $\Delta t = 15\,\mathrm{ps}$*

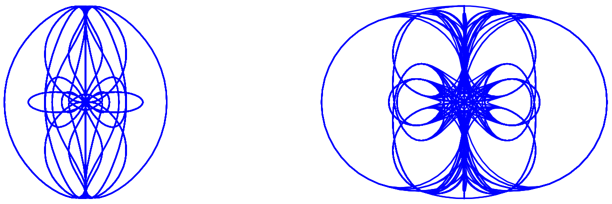

(d) *$\theta = 45^\circ$, $\Delta t = 5\,\mathrm{ps}$* ***(e)*** *$\theta = 45^\circ$, $\Delta t = 15\,\mathrm{ps}$*

Figure 4.11: *The Stokes representation of the signal, plotted in the S_1-S_2 plane.*

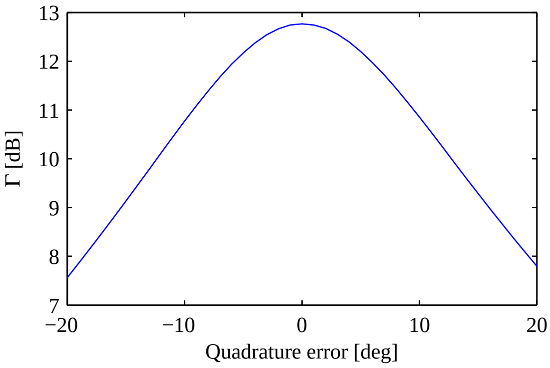

Figure 4.12: Γ *vs the quadrature error of the signal.*

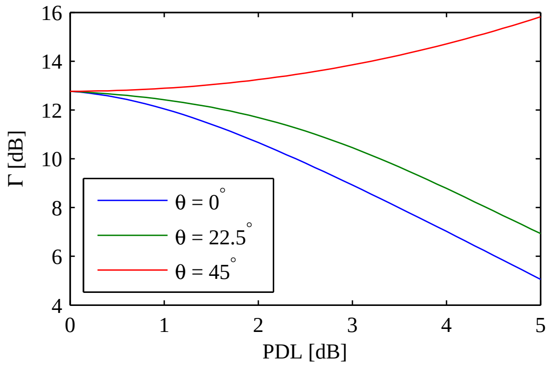

Figure 4.13: Γ *vs the power difference between the polarizations for different angles between the signal polarization and PDL axis.*

4.2.4 Other signal impairments

Also simulated were the effects of a quadrature error in the transmitter and polarization dependent loss (PDL). The Γ vs. OSNR curves can be seen in figures 4.12 and 4.13, respectively. For large values of both PDL and quadrature error the Γ values are severely affected. However, the quadrature error is generally controlled and kept at a low level in real systems. This is generally true for other transmitter impairments as well, such as bias errors, IQ gain imbalance and IQ-skew. The XY skew is equivalent to PMD aligned with the signal polarization, and from the results of the PMD simulations we know that this does not not affect Γ very much.

5 | Experiments

The experiments can be divided into two main parts, namely (i), those related to improving the polarimeter setup, and (ii), those related to investigating the performance of the method for measuring the OSNR. Both parts are presented in this chapter.

5.1 Polarimeter setup

The polarimeter setup used was nearly identical to the setup described in chapter 3, with fiber coupled components. The 90° hybrid used was a Kylia COH24 single polarization hybrid, and the balanced detectors were Newport 1817 80 MHz. As ADC, a TiePie Handyscope HS4 was used, at a sampling rate of 50 MHz. In addition, external filters with bandwidth $\Delta f = 10\,\text{MHz}$ were used.

To compensate for length differences between the connecting fibers of the two arms of the PBS, two variable optical delays were added. A delay between the two arms will act as a DGD element, giving the same effect as a fiber with PMD. A fiber length of 1 mm corresponds to 5 ps. This is equivalent to $0.14\,T_s$ for a 28 GBd signal, which degrades the results significantly. As the connecting fibers differed several centimeters, the variable delays were necessary. To find the right amount, the delay was adjusted manually to find the minimum of the disc thickness. Note that the compensation cannot be performed with digital signal processing, as this would require knowledge of the complete E_x and E_y. After the hybrid, only the low-pass filtered phase difference between E_x and E_y can be extracted.

In addition to the delay between the arms of the PBS, there was also a delay between the S_1, S_2 and S_3 channels. However, as this is in the electrical domain it is possible to compensate for with digital signal processing.

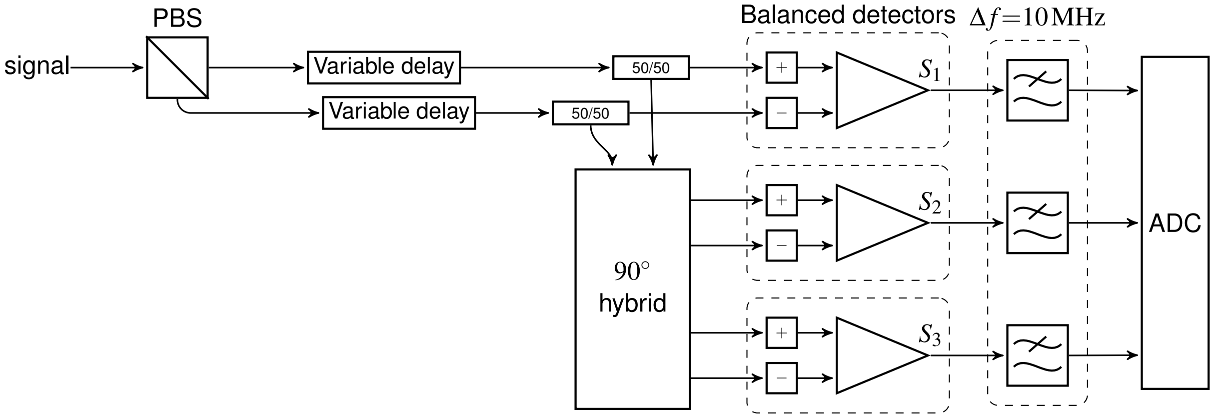

Figure 5.1: The polarimeter setup. The variable delays were added to compensate for length differences between the connecting cables.

5.1.1 Digital signal processing

The DSP includes retiming of S_1, S_2 and S_3, to compensate for different path-lengths, compensation for hybrid imperfections, and extraction of the dimensions of the disc. To be able to make smaller timing adjustments than the sampling time, the retiming was performed by interpolating the signals, using sinc interpolation.

Hybrid imperfections

As shown in chapter 3, a non-ideal hybrid can be represented by the matrix equation

$$\mathbf{S}' = \begin{pmatrix} S'_0 \\ S'_1 \\ S'_2 \\ S'_3 \end{pmatrix} = \begin{pmatrix} \ell_{00} & 0 & 0 & 0 \\ \ell_{10} & \ell_{11} & 0 & 0 \\ \ell_{20} & \ell_{21} & \ell_{22} & 0 \\ \ell_{30} & \ell_{31} & \ell_{32} & \ell_{33} \end{pmatrix} \begin{pmatrix} S_0 \\ S_1 \\ S_2 \\ S_3 \end{pmatrix} = \mathbf{LS}, \tag{5.1}$$

where $\mathbf{S}$ is the real Stokes parameters and $\mathbf{S}'$ is the measured Stokes parameters. If we assume that S_0 is constant, these parts can be handled by removing the mean. This is equivalent to a DC-block.

The remaining matrix can be viewed as the product of a shear matrix and a scaling matrix. Thus

$$\begin{pmatrix} S'_1 \\ S'_2 \\ S'_3 \end{pmatrix} = \begin{pmatrix} \ell_{11} & 0 & 0 \\ \ell_{21} & \ell_{22} & 0 \\ \ell_{31} & \ell_{32} & \ell_{33} \end{pmatrix} \begin{pmatrix} S_1 \\ S_2 \\ S_3 \end{pmatrix} \tag{5.2}$$

is equivalent to

$$\begin{pmatrix} S'_1 \\ S'_2 \\ S'_3 \end{pmatrix} = \begin{pmatrix} \ell_{11} & 0 & 0 \\ 0 & \ell_{22} & 0 \\ 0 & 0 & \ell_{33} \end{pmatrix} \begin{pmatrix} 1 & 0 & 0 \\ \ell'_{21} & 1 & 0 \\ \ell'_{31} & \frac{1}{\tan\alpha} & 1 \end{pmatrix} \begin{pmatrix} S_1 \\ S_2 \\ S_3 \end{pmatrix}, \tag{5.3}$$

where the fact that $\ell_{32} = k\cos\alpha$ and $\ell_{33} = -k\sin\alpha$ have been used. The angle α corresponds to the phase shift in the hybrid, and should ideally be $\pi/2$.

The parameters could in theory be found by measuring the individual loss coefficients of the hybrid, but this proved to be hard. Instead, the parameters were found by fitting measurements to a sphere by adjusting the parameters. Two methods were used. The first used continous wave, single polarization light as input, which is represented by a single point on the Poincaré sphere. The polarization was scrambled, which together with the phase fluctuations in the polarimeter gave measurements that covered the whole sphere. In figure 5.2 the effect of the compensation on single polarization measurements is shown. The second method used the effect of the hybrid on the shape of the disc, with a DP-QPSK signal. To find the scaling factors, the assumption was made that the scaling could be compensated for before the shear by normalizing the coordinates of all measurements combined, so that they roughly form a sphere. As the hybrid imperfections distorts the disc depending on the direction it takes, giving a higher variation of the values, the shear parameters can be found by minimizing the variance of several Γ measurements. This effect can be seen in figure 5.3. Both methods produced similar results.

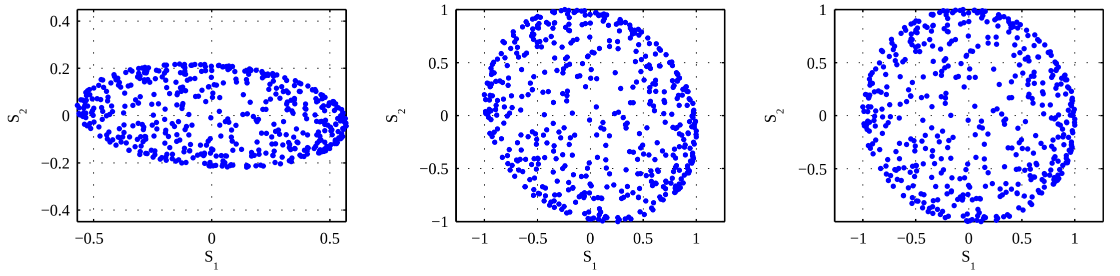

(a) No compensation

(b) Normalization

(c) Normalization and shear compensation

Figure 5.2: *Single polarization measurements, with random polarization state in the S_1-S_2-plane. Ideally the points should fill the circle, as the plot is the projection of a sphere.*

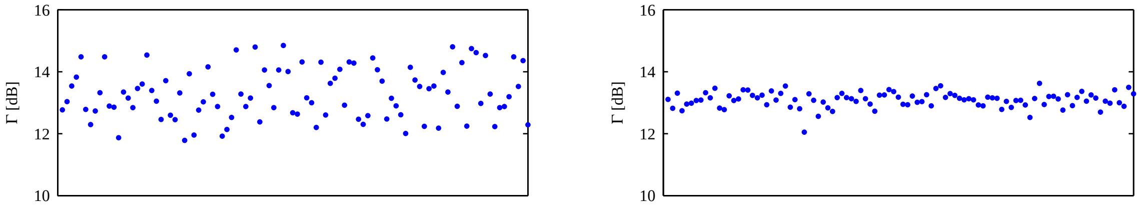

(a) Normalization only

(b) Normalization and shear compensation.

Figure 5.3: *Each point represents the Γ value for a single measurement, and the two plots illustrate the necessity of correcting for the hybrid imperfections.*

5.2 OSNR measurements

5.2.1 Transmitter setup

The polarization multiplexed signal was created by splitting a QPSK signal with a 3 dB coupler and delaying one of the arms with a length of fiber, shown in figure 5.4. This is the customary way of creating a DP-QPSK signal in the lab, without using two QPSK modulators. As a fixed length of fiber was used, the delay could not be adjusted. This resulted in the signal having a constant XY-skew. However, in chapter 4 it was shown with simulations XY-skew shifted Γ a fraction of a dB, so the created signal was still useful to test the system.

The data used was a PRBS with length of $2^{31}-1$, which was the longest sequence available with the pattern generator used. Generally, it is desirable to use a long PRBS since they are more similar to real signals with random data. As was discussed in section 4.2.1, it is also important that the spacing between frequency components of the signal is significantly smaller than the bandwidth of the system. Using Eq. (4.4), the spacing of PRBS31 is found to be $\Delta f_{PRBS} = 13\,\text{Hz}$. As the system bandwidth is $\Delta f = 10\,\text{MHz}$, the frequency components of the PRBS is not a limiting factor.

The noisy signal for the OSNR measurements was created by noise loading, i.e. adding noise to a noiseless signal. This was accomplished by combining the DP-QPSK signal with ASE from an EDFA without input signal. The OSNR was varied using a variable attenuator to control the noise power. An additional EDFA

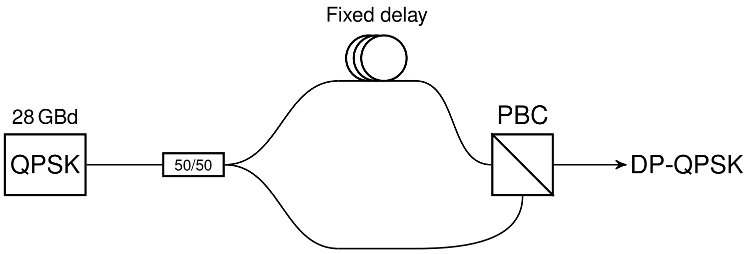

Figure 5.4: *The setup used for creating the dual polarization signal. Due to the fact that a fixed length of fiber was used as a delay, a constant XY skew was always present.*

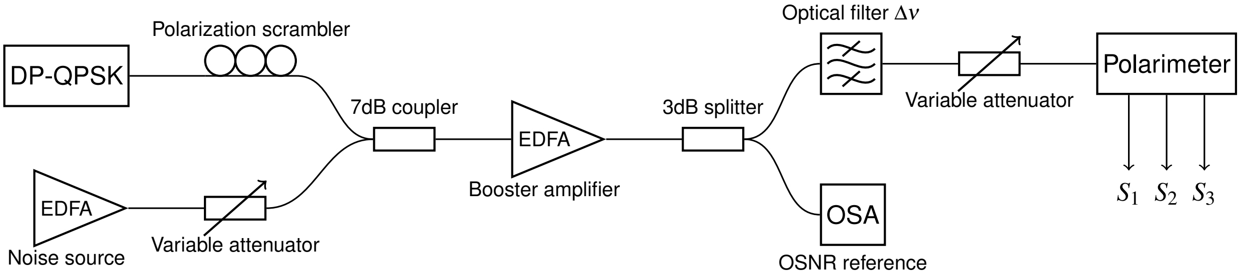

Figure 5.5: *The setup used for OSNR measurements.*

was then also used to boost the signal power. To make a reference measurement of the OSNR, the conventional optical spectrum analysis technique was used. This was possible since only one channel was present, and the reference was measured before the optical filter. After the optical filter, a variable attenuator was used to control the input power to the polarimeter.

The measurements were made with the polarization scrambled. This can be considered a worst case scenario, as the polarization of the signal in real systems varies in the fiber. Combined with the fact that the method also makes it possible to measure the angle of the input polarization, it also provides an easy way to find any polarization dependency of the Γ measurements.

5.2.2 OSNR estimation

To extract the OSNR value from the Γ measurements, the theoretical model of the relation between OSNR and Γ developed in chapter 3 was used. It should be noted that the inverse relation,

$$OSNR(\Gamma) = \frac{-k_1(1-\Gamma) + \sqrt{k_1^2(1-\Gamma)^2 - 4k_0(k_{22}-k_{21}\Gamma)(1-\Gamma)}}{2(k_{22}-k_{21}\Gamma)}, \tag{5.4}$$

has a very steep slope for values of Γ close to the maximum. This means that for high OSNR values, even small uncertainties in the Γ measurements will give rise to high deviations in the estimated OSNR. Another important feature of the relation (5.4) is that it has a singularity for $\Gamma = k_{22}/k_{21}$, where it approaches infinity. This point is equivalent to the maximum Γ value. For higher Γ values it has no practical significance, and takes negative values. However, as the measured values fluctuates, it is possible to get Γ measurements that exceeds the maximum when measuring high OSNR values. These measurements has to be discarded, or assumed to be the maximum measurable OSNR.

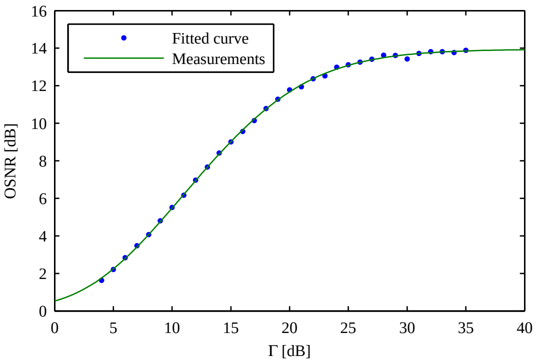

Figure 5.6: *The measured* Γ *vs. measured OSNR, together with the fitted theoretical curve.*

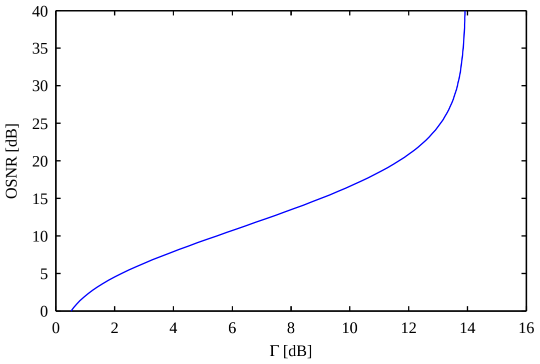

Figure 5.7: *The OSNR as a function of* Γ*. Note the steep slope for high OSNR values, and the vertical asymptote at* $\Gamma = 14\,\mathrm{dB}$*, which is the value of* k_{22}/k_{21} *for this particular case.*

The coefficients k_0, k_1, k_{21} and k_{22} were found using least-squares fitting to the measured values. In figure 5.6 the theoretical curve is plotted together with measurements. Here the values used were $k_0 = 113$, $k_1 = 72.8$, $k_{21} = 1$ and $k_{22} = 24.8$.

There was always a small variation between consecutive Γ values, so to get a more stable measurement, ten values were averaged. In figure 5.8 the estimated OSNR is plotted vs. the OSNR measured with the OSA. The estimated OSNR value keeps within the ±1 dB borders for reference OSNR values up to more than 25 dB. This can be considered a good result, as typical OSNR values are in the range of 15–20 dB. In both figure 5.8a and figure 5.8b the coefficients of Eq. (5.4) were fitted to the data in figure 5.8a. The OSNR estimation in figure 5.8b is obviously less accurate, which indicates that the result is sensitive to the values of the coefficients. However, by accident the polarization scrambler was turned of when the measurements in figure 5.8b were made. As there is a slight polarization dependence on the results (discussed below) this could be the reason for the deviation. Still, the measurements stability over time needs to be investigated.

To test the effect of chromatic dispersion the signal was transmitted through a length of 41.1 km single mode fiber with $D = 17\,\mathrm{ps/nm/km}$. However, no effect could be seen, which is consistent with the simulation results, predicting that measurements with a bandwidth of 10 MHz should tolerate at least 1000 km of fiber. The estimated OSNR from the measurements with the fiber can be seen in figure 5.9. The coefficients used to estimate the OSNR were fitted to the data from another measurement, which explains the deviations for higher OSNR values.

As previously mentioned, the uncertainty in the OSNR estimation grows for higher OSNR values. To investigate this, 500 measurements were made for OSNR values of 15, 20 and 25 dB. The result is plotted in figure 5.10a. On the x-axis is the angle of the disc normal to the S_1 axis, representing the polarization of the signal relative to the polarimeter. In this graph a slight polarization dependence of the OSNR values can be seen. This could be caused by the hybrid compensation not being perfect or a remaining delay between the inputs of the hybrid. If the polarization of the signal is varying rapidly, an error like this is mitigated by taking an average of several measurements, but for a stable polarization it could be a source of errors.

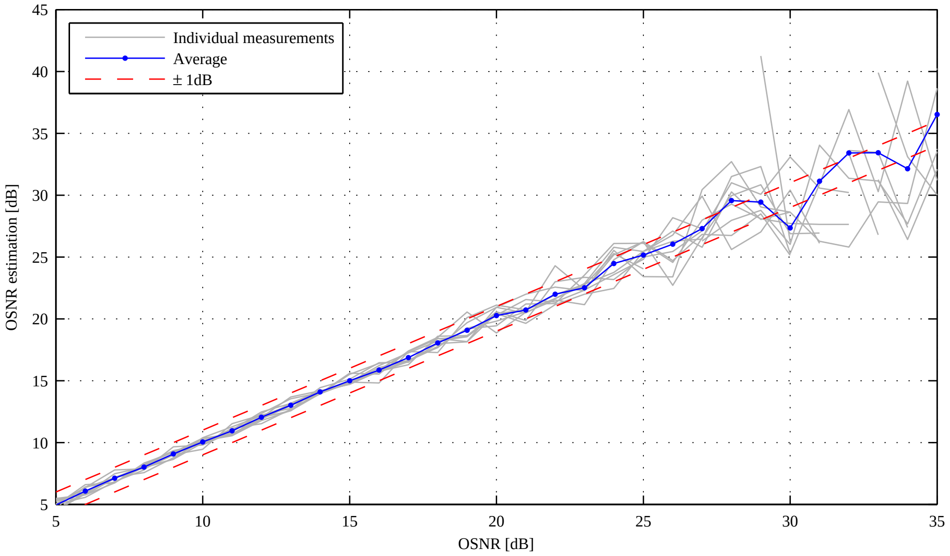

(a)

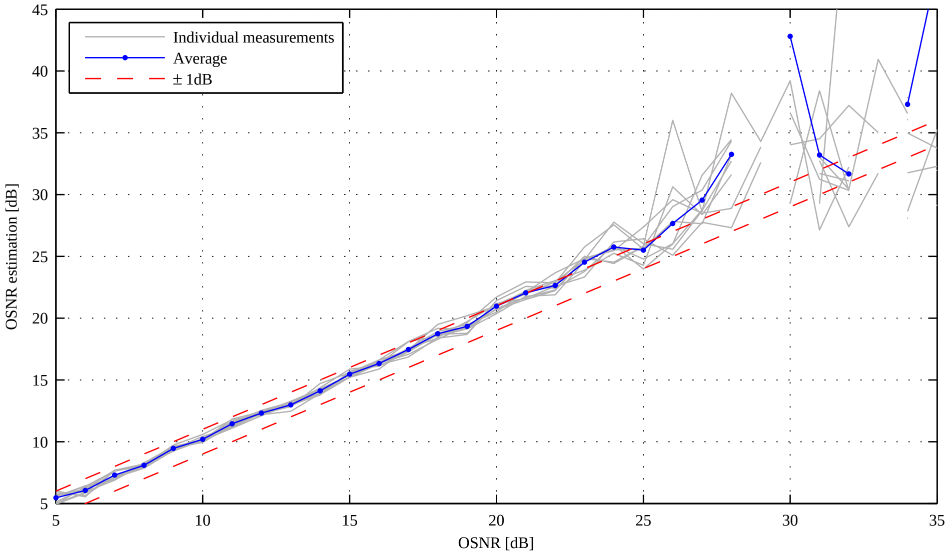

(b)

Figure 5.8: *The estimated OSNR vs. the OSNR measured with the OSA. Both the individual measurements and the average is plotted. The unconnected line segments for large OSNR values are because of* Γ *values higher than* k_{22}/k_{21}*, which were simply omitted from the plot. Figure (a) and (b) show different measurements, but the theoretical model was fitted to the data in (a). The fact that the curve in (b) is less accurate than the one in (a) is an indication that the result is sensitive to variations in the coefficients in the model.*

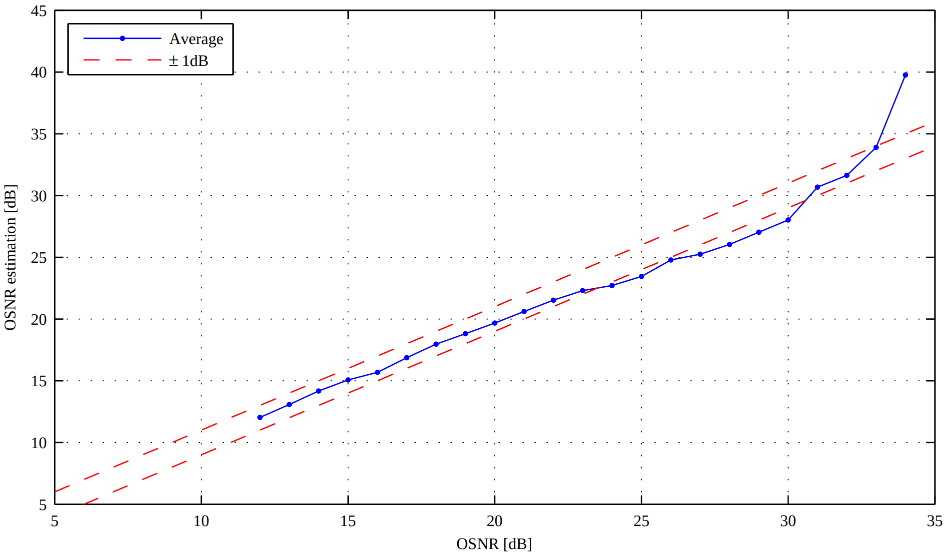

Figure 5.9: *The estimated OSNR vs. the OSNR measured with the OSA, with the dispersion from a 41.1 km SMF.*

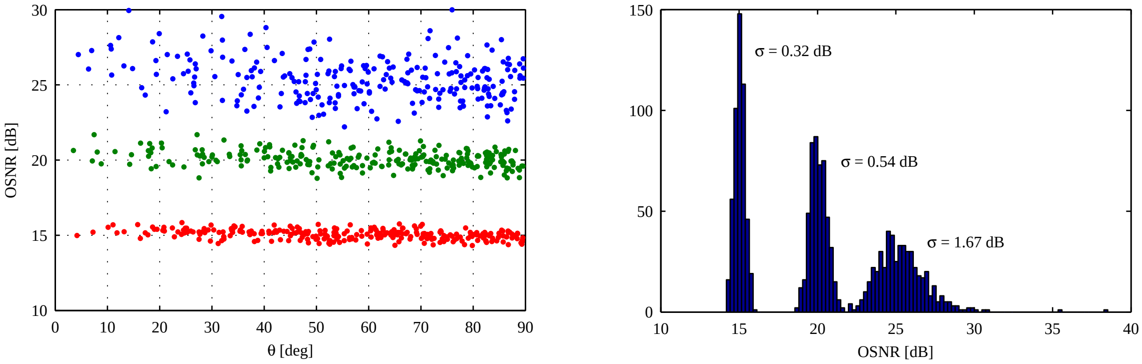

(a) *500 Γ measurements, for 15, 20 and 25 dB. On the x-axis is θ, the angle between the disc normal and the S_1-axis.*

(b) *Histogram of the measurements in (a).*

Figure 5.10: *Two plots that illustrate the increase of measurement uncertainty with higher OSNR values.*

5.2.3 PMD

The effect of PMD was tested using a PMD emulator that introduced a variable DGD by splitting the signal in two orthogonal polarization states and delaying one of them. The signal polarization was scrambled before the PMD emulator, giving a random orientation of the DGD element. 500 measurements were made for a DGD of 3 ps, 6 ps and 9 ps, with a noise-free signal. The Γ values are plotted in figure 5.11. As predicted by simulations Γ is severely affected. With the DGD axis scrambled, this leads to a large variation of Γ as the effect depends on the angle between the signal polarization and the DGD element.

In figure 5.12 the Γ value for a noise-free signal is plotted vs. the DGD. The results are consistent with the ones in figure 5.11, and also reveals that up to a couple of picoseconds of DGD can be allowed for the 28 GBd DP-QPSK signal.

5.2.4 Other experiments

The effect of a quadrature error was also tested, and the result can be seen in figure 5.13. As for the simulations, the quadrature error does affect the Γ value, but as it is controlled in a real system, that is probably not a problem.

The setup worked for input power ranging between $-12\,\mathrm{dBm}$ and $-2\,\mathrm{dBm}$. The upper power limit was set by detector saturation and the lower by noise in the detectors. A way to increase the upper power limit would be to attenuate the inputs of the S_1 detector, which is saturated first. This could possibly also improve the lower limit, because the limiting factor is a larger variation in the Γ values due to the different impact of noise on S_1 as opposed to S_2 and S_3.

5.2.5 Comparison with simulation results

The results from the measurements show a good qualitative agreement with the simulations, with the same shape of the Γ vs. OSNR curves. A comparison of the simulated and measured curves can be seen in figure 5.14. The differences that can be seen are probably due to different electrical bandwidths and different pulse shapes.

As mentioned previously, the simulations suggested that the method should tolerate the dispersion from over 1000 km of SMF, but this could not be tested in the lab due to the lack of necessary equipment. However, the measurements showed that 41.1 km SMF had no effect on the result. Also investigated was the effect of PMD and quadrature error, which also showed a good qualitative agreement between simulations and measurements.

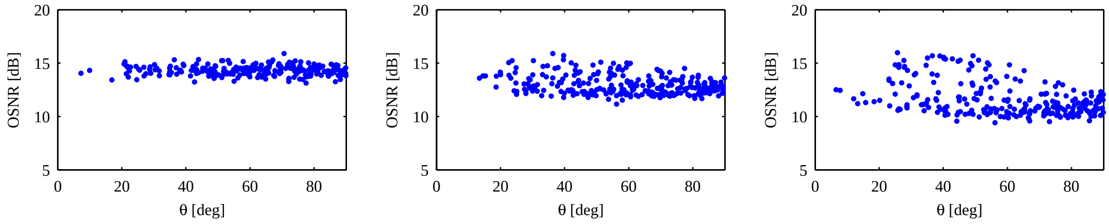

(a) $\Delta t = 3\,ps$ ***(b)*** $\Delta t = 6\,ps$ ***(c)*** $\Delta t = 9\,ps$

Figure 5.11: *Measured* Γ *values with different amounts of DGD. On the x-axis is* θ*, the angle between the normal of the disc and the* S_1*-axis.*

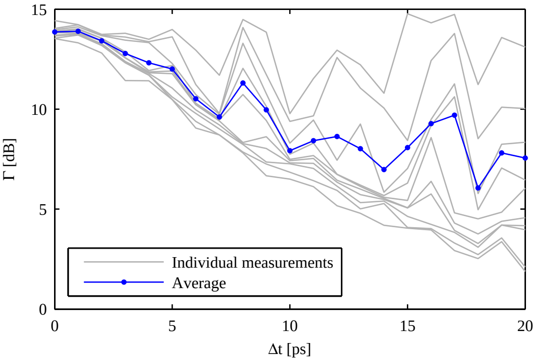

Figure 5.12: *The measured* Γ *value vs. the amount of DGD. Note that the main effect of increased DGD is a larger spread of the* Γ *values*

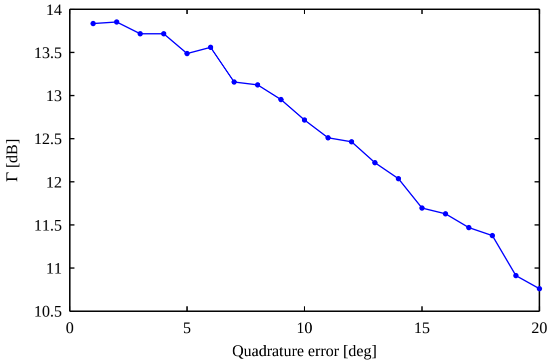

Figure 5.13: *The measured* Γ *vs. the amount of quadrature error.*

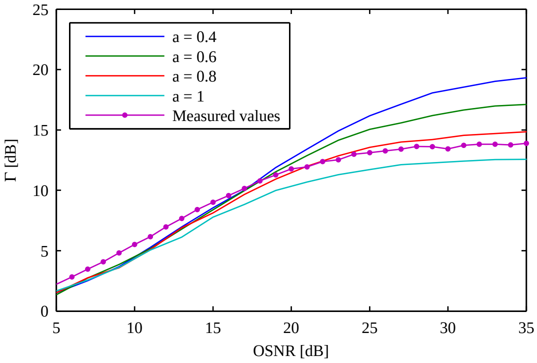

Figure 5.14: *A comparison between the simulated and the measured* Γ *vs. OSNR curves. The basic shapes of the curves are similar. The slight differences that can be seen are probably because of the differences in electric bandwidth,* $\Delta f = 1\,\text{GHz}$ *for the simulation and* $\Delta f = 10\,\text{MHz}$ *for the measurements, and differences in pulse shape. The parameter* a *is related to the rise time of the simulated raised-cosine pulses.*

6 | Conclusions

In this project, a 90°-hybrid-based polarimeter was constructed and evaluated as an OSNR monitor. With both simulations and measurements it has been demonstrated that the polarimeter successfully estimates the OSNR within ±1 dB for a 28 GBd DP-QPSK signal for OSNR values up to 25 dB. It has also been demonstrated that the method is insensitive to large values of chromatic dispersion.

It is not only possible to use a low bandwidth ADC, which is desirable for cost reasons, but a low bandwidth is also necessary to mitigate the effects of chromatic dispersion. The simulations suggested that a bandwidth of 10 MHz should allow for more than 1000 km of single mode fiber (SMF) transmission, and it was confirmed that 41.1 km of SMF did not affect the measurements.

However, PMD degrades the accuracy of the OSNR estimation severely for DGD values above a couple of picoseconds. The method is also sensitive to the pulse shape and spectrum of the signal.

With the goal of developing a practical, versatile OSNR monitoring method there are several aspects that need to be investigated further to improve measurement accuracy and long-term stability. The needed studies can be divided into three main categories, (i) further investigations of the effect of signal impairments and the compensation for these, (ii) the difference in the results for different non-faulty signals and (iii) testing of other hardware setups.

In this work, the effects of non-linearities in the fiber were not investigated. This was mainly because it requires either an extended simulation effort or testing equipment not available, but also because non-linearities are kept at a low level in real systems since they affect the overall system performance. Nonetheless, it is a topic that should be investigated.

One of the findings in this work is the sensitivity to PMD of the method. Even if the amount of DGD is low in modern systems, an important topic is to find a way of compensating for the PMD effects.

A topic that was only introduced briefly is that of the effect of different transmitter characteristics, and the sensitivity to errors in the calibration. A thorough investigation of this is needed to determine if the method needs to be calibrated to different transmitters. There is also a need for an investigation of the measurement stability over time.

The hybrid based-lumped component polarimeter used in this work has several disadvantages, for example the need for adjusting the delays after the PBS. The setup is also sensitive to vibrations due to the relatively long interconnecting fibers, which cause phase fluctuations and rotations of the disc. This problem could be avoided by using a completely integrated solution [4]. There are also several commercial polarimeter solutions available that could be evaluated for use for OSNR measurements, such as the Agilent N7781B, Thorlabs IPM5300 and General Photonics POD-101D.

Bibliography

[1] G. P. Agrawal, *Fiber-optic communication systems*, 4th ed. Hoboken, New Jersey: John Wiley & Sons, Inc, 2010.

[2] J. H. Lee and Y. C. Chung, "Optical signal-to-noise ratio monitoring," in *Optical performance monitoring: Advanced techniques for next-generation photonic networks*. Elsevier Inc., 2010.

[3] R. Schmogrow *et al.*, "150 gbit/s real-time nyquist pulse transmission over 150 km ssmf enhanced by dsp with dynamic precision," in *Optical Fiber Communication Conference and Exposition (OFC/NFOEC), 2012 and the National Fiber Optic Engineers Conference*, 2012, pp. 1–3.

[4] T. Saida *et al.*, "In-band OSNR monitor for DP-QPSK signal with high-speed integrated stokes polarimeter." Optical Society of America, 2012. [Online]. Available: http://www.opticsinfobase.org/abstract.cfm?URI=ECEOC-2012-Th.2.A.2

[5] "100G ultra long haul DWDM framework document," http://www.oiforum.com/public/documents/OIF-FD-100G-DWDM-01.0.pdf, June 2009, accessed October 2013.

[6] D. Gariépy, G. He, Y. Breton, B. D, and G. W. Schinn, "Novel OSA-based method for in-band OSNR measurement," in *Optical Fiber Communication Conference*. Optical Society of America, 2010.

[7] D. Gariépy, G. He, and G. W. Schinn, "Non-intrusive measurement of in-band OSNR of high bitrate polarization-multiplexed signals," *Optical Fiber Technology*, vol. 17, no. 5, pp. 518 – 522, 2011.

[8] S. Savory *et al.*, "Digital equalisation of 40gbit/s per wavelength transmission over 2480km of standard fibre without optical dispersion compensation," in *Optical Communications, 2006. ECOC 2006. European Conference on*, 2006, pp. 1–2.

[9] H. Hurwitz and R. C. Jones, "A new calculus for the treatment of optical systems," *J. Opt. Soc. Am.*, vol. 31, no. 7, pp. 493–495, Jul 1941.

[10] E. Hecht, *Optics*, 4th ed. Addison Wesley, 2002.

[11] B. Szafraniec, T. Marshall, and B. Nebendahl, "Performance monitoring and measurement techniques for coherent optical systems," *Journal of Lightwave Technology*, vol. 31, no. 4, pp. 648–663, 2012.

[12] L. Råde and B. Westergren, *Mathematics handbook*, 5th ed. Studentlitteratur, 2004.

[13] I. Söderkvist, “Using SVD for some fitting problems,” http://www.ltu.se/cms_fs/1.51590!/svd-fitting.pdf, 2009, accessed April 2013.

[14] D. C. Lay, *Linear algebra and its applications*, 3rd ed. Boston, Massachusetts: Pearson, Addison Wesley, 2006.